Lab on a Chip

CRITICAL REVIEW

View Article Online
View Journal | View Issue

Cite this: *Lab Chip*, 2017, **17**, 1406

Microfluidic neural probes: *in vivo* tools for advancing neuroscience

Joo Yong Sim,[a] Matthew P. Haney,[b] Sung Il Park,[c] Jordan G. McCall[def] and Jae-Woong Jeong[*bg]

Microfluidic neural probes hold immense potential as *in vivo* tools for dissecting neural circuit function in complex nervous systems. Miniaturization, integration, and automation of drug delivery tools open up new opportunities for minimally invasive implants. These developments provide unprecedented spatiotemporal resolution in fluid delivery as well as multifunctional interrogation of neural activity using combined electrical and optical modalities. Capitalizing on these unique features, microfluidic technology will greatly advance *in vivo* pharmacology, electrophysiology, optogenetics, and optopharmacology. In this review, we discuss recent advances in microfluidic neural probe systems. In particular, we will highlight the materials and manufacturing processes of microfluidic probes, device configurations, peripheral devices for fluid handling and packaging, and wireless technologies that can be integrated for the control of these microfluidic probe systems. This article summarizes various microfluidic implants and discusses grand challenges and future directions for further developments.

Received 31st January 2017,
Accepted 17th March 2017

DOI: 10.1039/c7lc00103g

rsc.li/loc

[a] *Electronics and Telecommunications Research Institute, Bio-Medical IT Convergence Research Department, Daejeon, 34129, Republic of Korea*
[b] *Department of Electrical, Computer, and Energy Engineering, University of Colorado Boulder, CO 80309, USA. E-mail: jaewoong.jeong@colorado.edu*
[c] *Center for Remote Health Science Technologies, Department of Electrical and Computer Engineering, Texas A&M University, College Station, TX 77843, USA*
[d] *Department of Anesthesiology, Washington University in St. Louis, St. Louis, MO 63110, USA*
[e] *Department of Pharmaceutical and Administrative Sciences, St. Louis College of Pharmacy, St. Louis, MO 63110, USA*
[f] *Center for Clinical Pharmacology, St. Louis College of Pharmacy and Washington University School of Medicine, St. Louis, MO 63110, USA*
[g] *Materials Science and Engineering Program, University of Colorado Boulder, CO 80309, USA*

1. Introduction

Understanding the human brain, which consists of billions of neurons and trillions of connections between diversified cell types, remains one of the greatest challenges in science and medicine. Our knowledge of the underlying mechanisms for how these complex systems function to promote natural behaviours and respond to disease states is still greatly limited. Our ability to advance this knowledge and address related clinical pathologies relies heavily on technological innovation. Recent collaborative research initiatives (*e.g.* BRAIN Initiative in the United States, the Human Brain Project in

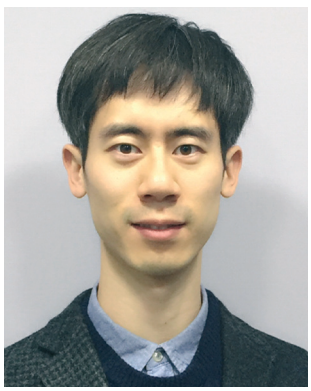

Joo Yong Sim

Dr. Joo Yong Sim received his BS degree in mechanical and aerospace engineering from Seoul National University and his MS and PhD degrees in mechanical engineering from Stanford University. Since then, he has been working as a researcher in the Electronics and Telecommunications Research Institute. His research is primarily in the area of biomedical engineering and biophysics focusing on the development of biomedical sensors and actuators using microelectromechanical systems, microfabricated devices, biophotonics and advanced microscopy technologies.

Matthew P. Haney

Matthew P. Haney is a graduate student in the Electrical, Computer, and Energy Engineering department at the University of Colorado Boulder. He received his BS degree in electrical engineering from the same institution in 2017 with focus on nano/micro materials and fabrication. He works and studies in Dr. Jae-Woong Jeong's research laboratory, where he specializes in the fabrication and characterization of soft biomedical devices.

Europe, Brain/MINDS of Japan, the China Brain Project, and others)[1–3] have sought to promote advances in neurotechnologies that can lead to dynamic and systematic understanding of how neurons and neural circuits interact in the brain. These efforts aim to understand fundamental neural function and provide clarity for a host of intractable psychiatric and neurological disorders. In line with this endeavour, researchers have investigated various electrical,[4–6] genetic,[7] and optical[8–11] techniques for dissection of complex neural circuits.

Microfluidic neural interfaces hold immense potential for basic neuroscience research and clinical medicine.[4,12–14] *In vivo* neuropharmacology enables delivery of pharmacological agents deep into the brain to help dissect complex neural circuits and neurotransmitter/receptor systems[15] and treat neurodegenerative diseases and brain tumors.[16] Recent studies show that pharmacological delivery can be combined with optical intervention for advanced optogenetic and chemogenetic manipulation of the brain,[14,17–24] light-regulated activation of pharmacological agents for high-spatiotemporal control of cellular activities,[25–27] as well as sophisticated deep brain stimulation for the treatment of psychiatric disorders.[23] Beyond traditional pharmacological agents, there is great potential for the successful delivery of other fluidic agents such as chemogenetic ligands,[22,28,29] gene therapy vectors[30] and antibody treatments for chronic diseases.[31] Therefore, the development of novel minimally invasive, multifunctional brain-interfacing microfluidic technologies is of the utmost importance for both basic neuroscience and clinical medicine. Despite this need, however, there have only recently been concerted materials and engineering efforts to overcome obstacles inherent to traditional fluid-delivery approaches. The most notable delivery-related challenges arise from the decades-old use of metal cannulas for pharmacological infusions. This conventional method has been effective for basic research to date but is not spatially precise at the scale relevant to brain microcircuits and is not suitable for long-term clinical intervention. The implanted metal tubes extensively damage the targeted brain region and nearby areas, are not optimized for pairing with concurrent optical or electrical manipulation/observation of neural activity, and severely limit the subject's range of motion due to its tethered operation. In other words, this technology lacks cellular-scale control of drug delivery and the multifunctionality to support wireless, concurrent optical and/or electrical neural stimulation and recording.

To overcome these limitations, innovative efforts combining neuroscience with engineering have been made to

Sung Il Park

Dr. Sung Il Park is an Assistant Professor at Texas A&M. Park earned his PhD in electrical engineering from Stanford University. His expertise is in soft neural interface, low power analog circuits, high frequency RF circuit and antenna, and wireless power/communications systems. He has served as a peer reviewer for Applied Physics Letters, IEEE Transaction on Biomedical Engineering and Progress in Electromagnetics Research. His recent work on soft, stretchable, fully implantable miniaturized optoelectronic systems for wireless optogenetics has been featured in Nature Biotechnology and several news agencies.

Jordan G. McCall

Dr. Jordan G. McCall is an Assistant Professor at the Center for Clinical Pharmacology in the Department of Anesthesiology at Washington University in St. Louis School of Medicine and Department of Pharmaceutical and Administrative Sciences at St. Louis College of Pharmacy. He received his BA, BS, and MPH degrees from the University of Missouri-Columbia and his PhD degree in neurosciences from Washington University in St. Louis. Dr. McCall's laboratory studies the neural mechanisms of stress, chronic pain, and addiction. To work towards more effective treatments for these disorders, the laboratory is developing new technology to overcome existing limitations for accessing the nervous system.

Jae-Woong Jeong

Dr. Jae-Woong Jeong is an Assistant Professor in Electrical, Computer, and Energy Engineering and Materials Science and Engineering Program at the University of Colorado Boulder. He received his BS degree from the University of Texas at Austin and his MS and PhD degrees from Stanford University, all in electrical engineering. He is an inventor of the wireless optofluidic neural systems for in vivo pharmacology and optogenetics, which was published in Cell and Nature Protocols. Dr. Jeong's research laboratory focuses on the development of next-generation soft biomedical devices for fundamental neuroscience research and various clinical applications.

develop spatiotemporally precise tools for *in vivo* neuropharmacology (*i.e.* microfluidic neural probes).[4,14,32,33] Microfluidic neural probes greatly minimize neural tissue damage, enable delivery of multiple distinct pharmacological or otherwise fluid agents, and facilitate integration with various other modalities, such as optical, electrical, and/or chemical components within a single implant. Continued advances in materials, microfabrication, and integration technologies have led to unprecedented microfluidic tools with the potential for revolutionizing fundamental neuroscience and clinical medicine (Fig. 1). Many microfluidic probes are suitable for application in rodent behavioural neuroscience laboratories but could easily be extended to work in other species and biomedical disciplines as well. Therefore, these probes represent an extremely important and versatile technology to overcome current limitations and meet significant needs in brain research and therapy.

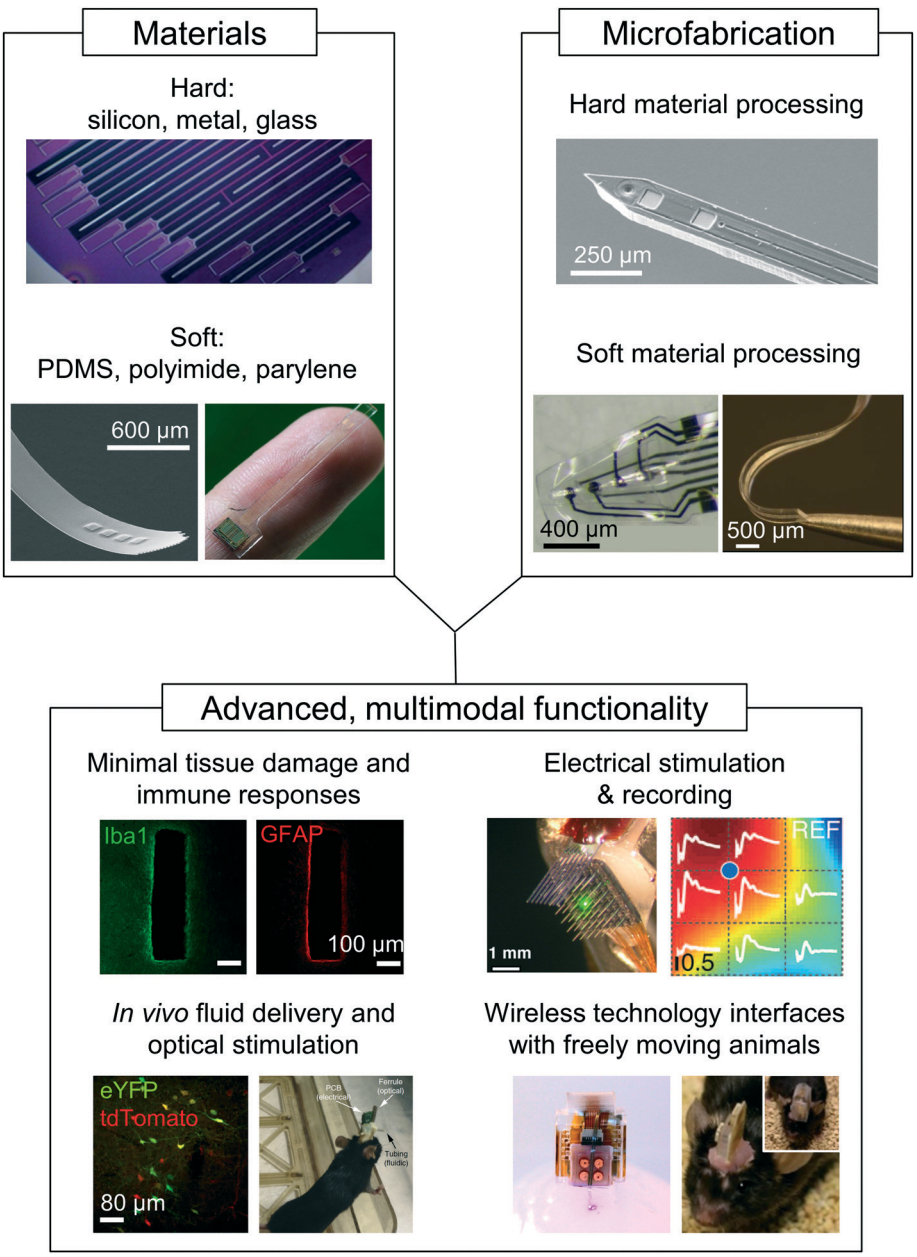

Fig. 1 Key design considerations in microfluidic neural probes. The choice of materials and the microfabrication scheme are critical components to be considered for the design of advanced, multimodal microfluidic neural probes. The materials can be categorized into hard materials, such as silicon and metal, and soft materials, such as PDMS, PI, and Parylene C.[69,73,91] The fabrication schemes highly depend on the characteristics of each material.[6,33,87] Integration of multimodalities for simultaneous pharmacological delivery, optical and electrical stimulation, and electrical recording can provide versatility for various applications.[4,5,14,32] Advanced microfluidic neural probes combined with wireless technology will ultimately help minimize tissue damage and immune response, ensure freedom of movement and behaviour, and enable wireless manipulation of neural circuitry using *in vivo* pharmacology, electrophysiology, optogenetics, and optopharmacology.[14]

Overviews of electrical or optical neural probe technologies were reported previously in terms of their fabrication and applications.[34–36] More recent review papers outlined state-of-the-art electrical neural probes from the perspective of efforts to enhance biomechanical compatibility and protect the quality of chronic electrophysiological recordings against gradual degradation over time.[37–40] Some of the topics in previous review papers on electrical or optical neural probes can also be applied to microfluidic neural probes, but the unique features and challenges of the microfluidic neural probe technology have not yet been reviewed. The microfluidic neural probe is a relatively new technology and necessitates careful consideration of its unique aspects such as integration of fluidic functionality and fluid handling. In this review, we provide an overview of recent advances in neural probe technologies specific to microfluidic features and discuss grand challenges and potential future developments. We begin with a discussion on the key requirements and material options for microfluidic neural interfaces. The subsequent sections describe the types of probes and basic process technologies for microfluidic channel formation. Building on these process technologies, recent developments in microfluidic neural probes are illustrated with an emphasis on materials used for the manufacturing of devices and their extensible functionalities. We also discuss peripheral yet essential technologies required for fluid pumping and packaging. The following section highlights the trend in *in vivo* neuropharmacology toward wireless microfluidics for applications in awake, freely behaving animals. Lastly, we discuss challenges associated with the long-term application of microfluidic neural probes *in vivo* including biofouling, risk of infection, and clogging. This review concludes with a discussion on future research directions for microfluidic neural probe technologies to advance neuroscience research and clinical applications.

2. Requirements and materials for microfluidic neural interfaces

For over a century, the use of metal cannulas has been the standard method in neuroscience for pharmacological infusions into the brain. Fig. 2 shows a representative conventional cannulation system. The basic concept for injecting a fluid into the brain region of interest involves a simple fluidic pump connected to an implanted metal tube (Fig. 2A–C).[14] This methodology is used in virtually every field of neuroscience. However, these types of regional infusions are limited for the following reasons: i) the relatively bulky and rigid metal tube (250–500 μm in diameter; $E \sim 200$ GPa) causes destruction and inflammation of brain tissue; ii) the sheer size and design of the cannulation system restricts localization of the injection site; and iii) the tethered tubing that connects to the animal significantly restricts free movement and the ability to receive infusions in more naturalistic environments.

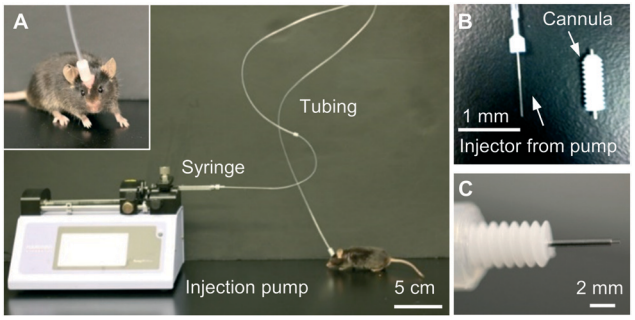

Fig. 2 Representative conventional cannulation system to deliver drugs into the brain. (A) A photograph of a conventional cannulation system, consisting of a simple fluidic pump connected to an implanted cannula (metal tube) for injecting a pharmacological substance into a brain region of interest.[14] The inset shows an awake, behaving mouse connected to the conventional tethered cannulation system. (B) The injector and metal cannula (0.5 mm diameter metal tube) and (C) the assembled injector/cannula for implantation into the brain. The injector can be seen extending 0.5 mm beyond the tip of the cannula.

To minimize invasiveness, ideal chronically implanted fluidic neural interfaces require both biological and mechanical compatibility with neural tissues as well as miniature dimensions (<100 μm). To satisfy these requirements, researchers have developed various types of microfluidic neural probes by combining novel materials and advanced microfabrication techniques. Material choice is particularly important because it determines the major characteristics of the microfluidic probe such as biocompatibility, elasticity, mechanical robustness, as well as the necessary fabrication processes. Stainless steel, fused silica, silicon, and polymers, such as polydimethylsiloxane (PDMS), Parylene C, SU-8, and polyimide (PI), are widely used due to their biocompatibility and well-established manufacturing processes. The key attributes of each material that define these characteristics are summarized in Table 1. In this review, we classify them into hard and soft materials, considering not only their mechanical properties but also their manufacturing processes – 'hard' materials ($E > 50$ GPa) include metals and inorganic materials such as stainless steel, fused silica, and silicon; 'soft' materials ($E < 10$ GPa) include various polymers such as PDMS, Parylene C, SU-8 and PI. More details about the basic fabrication processes for microfluidic channels using hard and soft materials are described in the next section.

Hard materials are classified by their rigidity, which does not offer local accommodation to micromotion or deformation of neural tissue. For example, stainless steel and fused silica, which are often used for metal cannula and glass capillaries, respectively, have a high modulus of elasticity (190–205 GPa for stainless steel;[41] 73 GPa for fused silica), resulting in stiff and rigid microfluidic probes. Silicon (130–170 GPa)[42] is another representative hard material that is broadly used for various types of microscale neural probes. The well-established processing methods for silicon, such as photolithography, wet/dry etching, and bonding techniques, enable researchers to manufacture almost any configuration

Table 1 Key properties of materials used as substrates for microfluidic neural probes, including stainless steel, fused silica, silicon, and polymers, such as PDMS, PI, Parylene C, SU-8 and COP

Properties of materials	Stainless steel	Fused silica	Silicon	PDMS	PI	Parylene C	SU-8	COP
Young's modulus (GPa)	190–205	73	130–170	$1–3 \times 10^{-3}$	2.5	2.2	4	1.7–3.0
Tensile strength (MPa)	480–620	50	7000	6.2	130	69	60	45–59
Poisson ratio	0.31	0.17	0.048–0.40	0.3–0.49	0.2	0.4	0.22	0.41
Biocompatibility (USP class)	—	—	—	VI	—	VI	—	—
Elongation (%)	40	<1	<1	600	10	200	6.5	—
Moisture absorption (%)	—	—	—	<1	2–3	0.06	0.55–0.65	<0.01
Thermal conductivity (W cm^{-1} K^{-1})	0.015	0.014	1.56	15–25	1.5	8.2	0.003	—
Thermal coefficient of expansion (ppm K^{-1})	17	0.5	2.6	—	12	35	52	60–70
Specific resistivity (Ω cm)	0.08	$>10^7$	10^{-4}–10^4	10^{15}	10^{16}	$>10^{16}$	$>10^{16}$	$>10^{16}$
Glass transition temperature (°C)	—	1000	—	—	>320	<90	200	70–163
Water vapour permeability[244,245] (Barrer, 30 °C)	Negligible	Negligible	Negligible	40 000	640	1.61	N/A	0.55
Reference	41	246	42 and 247	4, 14, 113, 245 and 248–251	45–49, 53, 55, 56 and 245	45, 50–52, 54 and 244	57–63	244, 252 and 253

and size of probe. These hard materials provide attractive options for constructing microfluidic probes because they are easy to handle and allow for high precision and high-yield production. However, the mechanical properties of these materials do not match those of biological tissues which can lead to neural tissue damage and inflammation.[43] This mechanical incompatibility raises questions about their suitability for long-term implantation.[44] Therefore, dedicated investigation will be necessary to engineer microfluidic probes that systematically address and overcome these limitations.

To address the challenges associated with hard materials, the scientific community has been investigating biocompatible soft materials for neural probes as a means to alleviate the mechanical mismatch between the tissue and the device. PI and Parylene C are widely used polymers for insulation and passivation of biomedical electronics. Both PI and Parylene C have low elastic moduli (2.5 GPa for PI[45–49] and 2.2 GPa for Parylene C[45,50–52]), high thermal and chemical resistances, and low moisture absorption rates, making them well-suited substrate materials for microfluidic neural probes.[48,52–55] The *in vivo* compliance of Parylene C has been demonstrated for permanent use as an implantable substrate by the United States Pharmacopeia (USP class VI).[52,54] While PI has not yet been approved for such an application, its biocompatibility has been demonstrated by multiple, distinct implantable devices.[48,56] Due to its photopatternability, SU-8, a negative photoresist based on epoxy, is another fascinating option for constructing flexible microfluidic probes. In the flexible category, SU-8 has a relatively high elastic modulus (4 GPa).[57–61] Therefore, it is possible to make flexible neural probes that still retain the rigidity required to penetrate the brain during the initial surgical insertion.[62] Although SU-8 does not satisfy all the requirements of the physiochemical biocompatibility test (*i.e.* ISO 10993-1),[63] numerous studies have demonstrated the *in vivo* and *in vitro* biocompatibility of this material.[62,64–67] PDMS, an elastomer-based polymer, is also one of the most widely used materials for medical devices with proven *in vivo* performance and compliance with the United States Pharmacopeia (USP class VI).[68] PDMS has a relatively low elastic modulus (~1 MPa) and large deformability (>600% elongation), which allows PDMS-based probes to conform to the dynamic deformation of biological organs.[69] Due to its high resistance to biodegradation and aging, PDMS has proven an effective substrate for many implanted devices, including bladder stimulators,[12] cardiac pacemakers,[70] and cochlear implants,[71] all of which suggests that this material has promise for use in chronic neural implants.

3. Types of microfluidic probes and basic process technologies

In this review, we classify microfluidic neural probes into stiff and flexible probes, depending on the moduli of elasticity of the probe materials. Ultrathin microfluidic probes made of hard materials can be flexible to some degree, but this class of probes is not sufficiently compliant to adapt to local deformation and movement of tissue. Here, we will classify stiff and flexible probes as being based on hard ($E > 50$ GPa; *e.g.* metal, silicon, glass) and soft materials ($E < 10$ GPa; *e.g.* polymers), respectively. Although stiff microfluidic neural probes include the traditional approaches of metal tubing and silica-fused capillaries, we focus on the fluidic neural interfaces miniaturized by the use of microfabrication technologies (*i.e.* microelectromechanical system (MEMS) technologies). The specifications and fabrication processes of both stiff and flexible microfluidic neural probes are summarized in Table 2. Stiff microfluidic neural probes use a hard substrate, frequently silicon, and fluidic channels can be formed on this substrate using various materials (*e.g.* silicon oxide,

Table 2 Summary of specifications and fabrication processes of stiff and flexible microfluidic neural probes

Substrate material	Process	Channel formation[a]	Structural material[a]	Additional functionality[b]	Channel dimensions	Probe dimensions	# of channels	Orifice opening	Tested range of differential pressure & flow rate	Flow resistance, kPa μl^{-1} min^{-1}	Operation	Ref.
Si	Surface	Sacrificial SiO*x*	Si, SiO*x*, SiN*x*	E	3 μm high 25 μm wide	100 μm thick 120 μm wide 2 mm long	1	30 × 15 μm	—	—	Tethered	78
	Surface	Sacrificial PR	Si, Parylene	E	10 μm high 50 μm wide 8 mm long	100 μm thick 100 μm wide 2–5 mm long	1	50–150 μm	7–310 kPa; 0.08–4.5 μl min^{-1}	70		79
	Bulk	XeF_2 etching	Si, Parylene	E	20 μm high 40 μm wide	100 μm thick 100 μm wide 2.8 mm long	4	5 × 5 μm	3–17 kPa; 1.5–10 μl min^{-1}	—		87
	Bulk	DRIE, isotropic etch	Si, poly-Si	S	ϕ 20 μm	70 μm thick 84 μm wide 11 mm long	2	ϕ 20 μm	—	—		90
	Bulk	DRIE, isotropic etch	Si, poly-Si	E	5–30 μm	200–380 μm thick 200–380 μm wide 15–70 mm long	2	5–30 μm	40–200 kPa; 0.02–1.6 μl min^{-1}	1000–5000		91
	Bonding	DRIE	Si	E	25 μm high 25 μm wide 8 mm long	150–250 μm thick 150 μm wide 8 mm long	1–4	ϕ 25 μm or 50 × 50 μm	0.5–2.5 kPa; 0.5–3.5 μl min^{-1}	**		82
	Bonding	DRIE	Si	E	50 × 50 μm	150–250 μm thick 150 μm wide 8 mm long	2–4	ϕ 25 μm or 50 × 50 μm	0.5–3 kPa; 0.5–5 μl min^{-1}	—		93
	Bonding	DRIE	Si, glass	E + M	10 μm high 5 μm wide* 11 mm long	40 μm thick	1	60 μm	50–120 kPa; 0.05–0.1 μl min^{-1}	—		81 and 94
PI	Bonding	Photolithography	PI	E	5–20 μm high 50–200 μm wide Centimeters long	—	4	30 × 30 μm or 50 × 50 μm	50–1300 kPa; 30–600 μl min^{-1}	—		112

Table 2 *(continued)*

Substrate material	Process	Channel formation[a]	Structural material[a]	Additional functionality[b]	Channel dimensions	Probe dimensions	# of channels	Orifice opening	Tested range of differential pressure & flow rate	Flow resistance, kPa μl^{-1} min^{-1}	Operation	Ref.
Parylene	Surface	Sacrificial PR	Parylene	E	10 μm high 50–200 μm wide	20 μm thick	1	50 × 10 μm	—	—		106
	Bonding	Molding, etching	Parylene	E	15 μm high 80 μm wide 7 mm long	18 μm thick	1	100 × 100 μm	0.5–7 kPa; 0.1–2 μl min^{-1}	5		107
SU-8	Bonding	Photolithography	SU-8	E	20 μm high 40–50 μm wide	55 μm thick 150 μm wide	1–2	ϕ 40 μm	10–140 kPa; 2.5–40 μl min^{-1}	—		67
PI, SU-8	Bonding	Photolithography	PI, SU-8	E	40 μm high 80 μm wide	240 μm wide 86 μm thick	2	ϕ 80 μm	Up to 60 μl min^{-1} at 1500 kPa	—		110
PDMS	Bonding	Molding	PDMS	E	50 μm high 150 μm wide	120 μm thick 3.2 mm wide 30 mm long	1	50 μm high 150 μm wide	40–80 kPa; 120–400 μl min^{-1}	14		4
	Bonding	Photolithography	PDMS	O	10 μm high 10 μm wide	80 μm thick 500 μm wide 6 mm long	4	10 μm high 10 μm wide	Up to 5 μl min^{-1}	—	Wireless	14
PC, COC	Thermal drawing	—	PC, COC	E + O	ϕ 200 μm	ϕ 400–700 μm	1–2	ϕ 200 μm	0.06–6 μl min^{-1}	—	Tethered	32

[a] PR: photoresist, Si: silicon, SiO*x*: silicon oxide, SiN*x*: silicon nitride, PC: polycarbonate, COC: cyclic olefin copolymer. [b] E: electrical recording, S: fluidic sampling, M: fluidic mixing, O: optical stimulation. *5 parallel channels, **1.5 μl min^{-1} at 1 kPa.

polymers). Silicon-based stiff microfluidic neural probes provide diverse and compelling options for *in vivo* pharmacology in neural tissue. However, these approaches are not ideally suited for chronic implantation because of the inflammatory

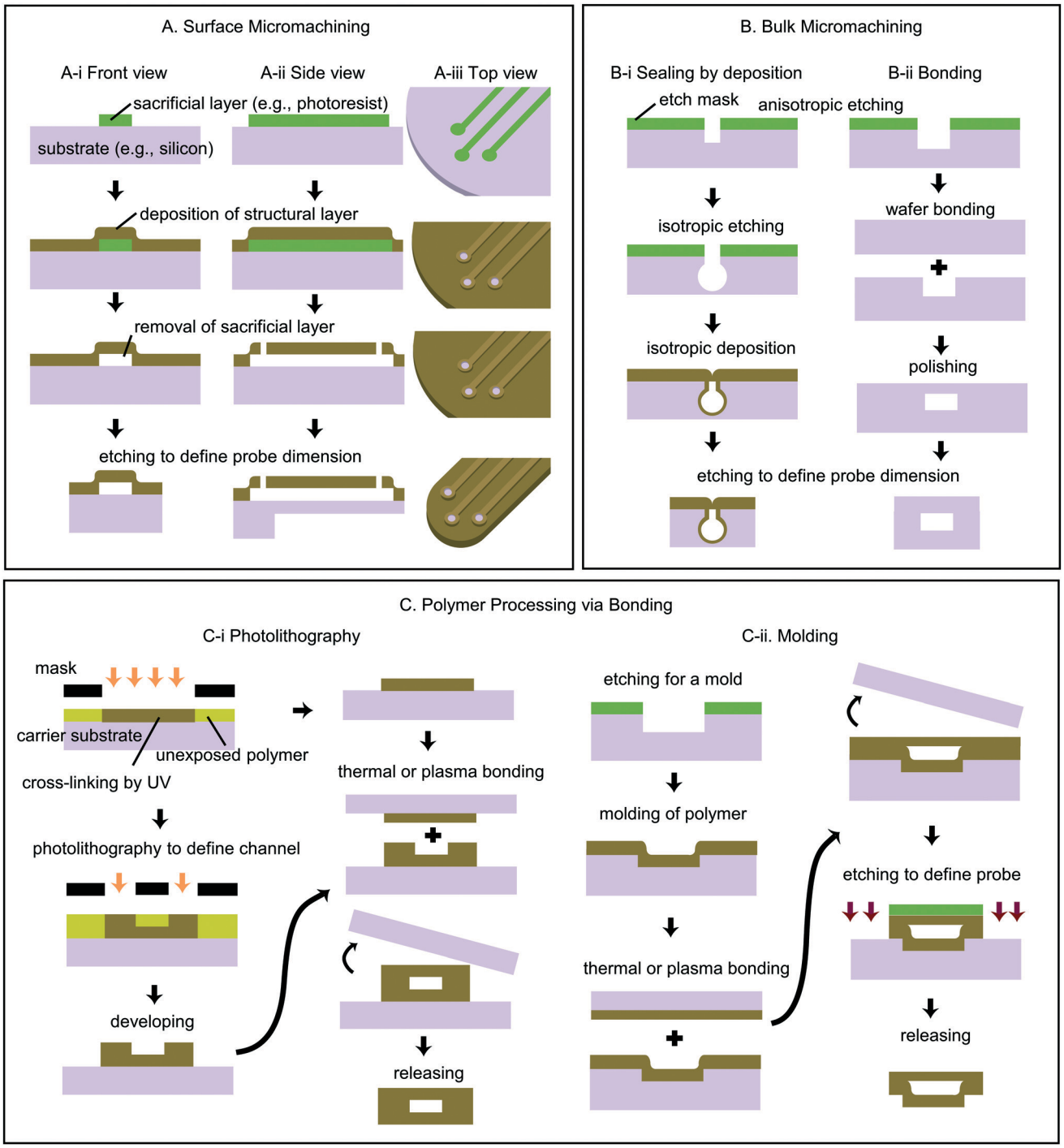

Fig. 3 Schematic diagrams of representative fabrication processes of microfluidic neural probes. Processes of (A) surface and (B) bulk micromachining, and (C) polymer processing *via* bonding. (A) The process steps of surface micromachining are illustrated in the front (A-i), side (A-ii) and top (A-iii) views: 1) deposit a sacrificial material (*e.g.* silicon nitride,[76,78] silicon oxide,[78] metals,[75,77] or polymers[79]), 2) cover the sacrificial layer with a structural material (*e.g.* metal,[75] silicon nitride,[76,78] silicon oxide,[78] or Parylene C[79]), 3) remove the sacrificial layer, and 4) etch to define the probe dimensions. (B) Two methods of defining and sealing the microchannel in bulk micromachining: (B-i) depositing isotropically grown materials and (B-ii) boding of another substrate. (C) Fabrication processes of polymer-based microfluidic neural probes *via* bonding. Prior to bonding of the top cover layer, the microchannels are constructed on a rigid carrier substrate (*e.g.* silicon wafer,[14,67,106,107,110,112] polyester,[110,112] or glass substrate[14]) by using (C-i) photolithography or (C-ii) molding. After forming the channel structure and defining the probe shape, the device is released from the carrier substrate.

responses mounted by microglia and astrocytes to the stiff structures.[44] Although proven effective for short-term applications, the mechanical mismatch between the soft brain tissue (E = 0.1–6 kPa) and the silicon probes (E = 130–170 GPa) can cause the formation of glial scars or neuron death around the implant.[72] Furthermore, the stiff neural probes implanted in the brain cannot accommodate micromotions that arise from locomotion and cardiorespiratory activities. Therefore, these stiff probes can cause continued, long-term tissue damage and inflammation. Both lesioning and inflammation can be problematic for chronic use as each confounds interpretations of behavioural effects compared to pharmacological treatment of the same region. Furthermore, glial activation and migration can contribute to both electrical and fluidic device failure. Experimental and theoretical analyses have shown that more mechanically compliant neural probes not only induce less strain on neural tissue but also enable neuron survival around the implantation site.[14,44,73] These outcomes provide motivation to develop polymer-based soft, flexible neural probes to replace or complement neural probes based on hard materials. In contrast to hard material-based probes, the excellent mechanical biocompatibility of flexible probes creates exciting prospects for minimally invasive neural implants. However, flexible probes have their own limitations. Flexible microfluidic probes are often unable to penetrate brain tissue on their own, requiring additional support in the form of a temporary scaffold made from a stiffer material. Due to differences in material properties, stiff and flexible microfluidic neural probes require different fabrication approaches. The following two sections describe the basic differences in these fabrication processes.

3.1. Fabrication of stiff microfluidic neural interfaces based on silicon

Adoption of well-established technologies for MEMS sensors and actuators has accelerated the miniaturization of fluidic neural interfaces. The mechanical characteristics of silicon allow for robust fabrication processes and numerous design schemes to precisely control the dimensions of the device on the microscale. Manufacturing with silicon also enables the creation of various types of stiff probes that are easily scalable and utilize established silicon microelectrode technologies. Therefore, microfluidic neural probes built with a silicon substrate provide diverse and compelling options for *in vivo* pharmacology in neural tissue.

Silicon MEMS fabrication techniques for microfluidic channel formation are divided into surface micromachining and bulk micromachining methods.[74] Fig. 3A and B show schematics of the representative processes of surface micromachining and bulk micromachining. Surface micromachining is based on sequential deposition and etching of multiple thin film and sacrificial layers, while bulk micromachining etches a bulk silicon substrate to create fluidic channels. In the case of surface micromachining, sacrificial materials (*e.g.* photoresists, silicon oxide) are used to define the channel geometry (Fig. 3A).[75–79] To construct the top layer of the channel, the sacrificial materials are subsequently covered by depositing structural materials such as silicon nitride,[76,78] silicon oxide,[78] metals,[75,77] and polymers.[79,80] The enduring temperature of the sacrificial material, the processing temperature of the structural material, and the etching compatibility of the two materials limit the selection of the structural material. To remove the sacrificial material, etch openings can be patterned onto the top cover layer along the channel length, allowing access to sacrificial materials for etch removal. These etch openings are used to make the etching duration of the sacrificial layer shorter and independent of the channel length.[76] After the sacrificial layer has been removed, the etch openings are sealed by isotropic deposition of the same or other structural materials (*e.g.* metal,[75] silicon nitride,[76,78] silicon oxide,[78] and Parylene C[79]). The mechanical robustness of the cover layer is important to maintain the structural integrity of the channels. In bulk micromachining, the channel structures are obtained by a wet etching or dry etching process, such as deep reactive ion etching (DRIE)[81,82] (Fig. 3B). The size of the etched trench structure determines the shape and dimensions of the microfluidic channel. The top openings are subsequently sealed by depositing isotopically grown materials[83–91] or by bonding the patterned material to another substrate.[81,82,92–94] DRIE etching of deep and narrow trench openings followed by isotropic dry etching can also create fluidic channels with relatively small top openings, thereby greatly facilitating the sealing of the channels.[83,85,86,89,91] In these fabrication processes, the sealed microchannel must be able to endure at least the maximum operating pressure of the device without rupturing (typically less than 2 bar). Reports in the literature demonstrate that microfluidic channels sealed by silicon wafer bonding[82] or adhesive PI bonding[95] can endure the maximum fluid pressure larger than 9 bar and 18.8 bar, respectively.

In both surface and bulk micromachining, the final dimensions of a device shank are determined by topside and backside etching using a DRIE process. The device thickness can vary from 40 to 400 μm and the length from 2 mm to 70 mm[91] as summarized in Table 2. In this final process, the top side of the device can be protected by a support wafer bonded with temporary adhesive during backside etching because the top side structure is delicate and prone to damage.[93] Alternatively, a microfluidic probe with cross-sections thinner than 20 μm can be achieved using silicon-on-insulator wafers whose insulator layer works as an etch stop to allow precise control of device thickness. Together, these two approaches to micromachining offer distinct considerations for the fabrication of stiff fluidic interfaces.

3.2. Fabrication of flexible microfluidic neural interfaces based on polymers

Various biocompatible polymers, including SU-8, PI, Parylene C, and PDMS, have been explored as substrates for flexible optical and/or electrical neural probe devices.[6,66,96–103] To

this aim, researchers are actively using these polymers to create ultrathin probe structures with embedded microfluidic channels.[4,14,33,67,104–109] To construct such ultrathin 3D channel structures, a variety of manufacturing schemes have been proposed for different polymers. Similar to silicon surface micromachining processes (Fig. 3A), flexible microfluidic neural probes can be fabricated using photoresist-assisted processing.[106] Another popular method to construct the cover layer of the microchannel using soft materials is thermal or plasma bonding (Fig. 3C).[107]

The photoresist-assisted method uses a channel-shaped sacrificial photoresist as a temporary positive mould, which is defined on a flat polymer film substrate. After coating another layer of polymer on the photoresist mould, the sacrificial photoresist can be dissolved and removed by solvent (*e.g.* acetone) to empty the channels. Etch holes are not typically made in the structural polymers due to their low modulus of elasticity. This approach is effective, but dissolution of the photoresist in thin, long channels is time-intensive. In addition, many flexible materials require an adhesion promoter to form a strong bond between the top and bottom layers, which makes this procedure cumbersome due to the incompatibility of the solvent for the adhesion promoter with photoresists.

The problems associated with the photoresist-assisted technique can be resolved by using thermal or plasma bonding (Fig. 3C). Prior to the bonding of the cover layer, the microchannel structures are constructed using either photolithography (SU-8,[62,66,67,110] photopatternable PI[105,110]) or moulding of the structural materials (Parylene C,[107] PDMS[4,14,33]). For example, SU-8 and photosensitive PI are photopatternable materials. Therefore, probe shape and the embedding of microfluidic channels in the device can be defined using standard UV photolithography (Fig. 3C-i). Both materials require multiple stacks of patterned polymer for the top, bottom, and walls of the channels. The bottom layer and intermediate channel walls are prepared by photolithography and then covered and sealed with a top SU-8 or PI layer by adhesive bonding (pressure: ~300 kPa; temperature: 100 °C for 20 min for SU-8,[67] and 300 °C for 60 min for PI[105]). The sealing *via* these bonding methods is strong enough to resist working pressure for infusion. A maximum operation pressure larger than 20 bar has been reported for a PI-based neural probe.[105] Parylene C is another attractive material, which can be conformally deposited on structured surfaces and patterned with oxygen plasma etching (Fig. 3C-ii). For the fabrication of microfluidic probes, Parylene C is conformally coated on a negative channel structure and a flat substrate. Subsequently, thermal bonding is made to create a robust fluidic channel structure (*e.g.* thermally bonding two Parylene C layers together in a 160 °C oven for 30 min under a bonding pressure of ~5 MPa[107]). After constructing the microchannels, the flexible microfluidic probe is released from a rigid carrier substrate (*e.g.* glass or silicon wafer). The adhesion between the probe and the carrier substrate has to be strong enough to resist shear forces during the etching and washing processes and to prevent the probe from peeling off. However, it is also important to easily detach the flexible probe from the carrier substrate without damaging the probe during this final release. To facilitate this step, a sacrificial layer can be deposited on a hard carrier substrate prior to the deposition of the polymer. For instance, aluminium can be deposited to release a Parylene C probe by dissolving the aluminium layer in a sodium chloride solution in the final peeling step.[107] Polystyrene sulfonic acid can be also used as a water soluble release layer on a carrier wafer, which helps to release flexible microfluidic neural probes from the carrier wafer upon a brief immersion in water.[4] For PDMS probes, a Pt inhibitor can facilitate release of probes from the glass slide by inhibiting polymerization of PDMS at the glass–PDMS interface.[14] These approaches demonstrate the necessary use of sacrificial materials in the fabrication of flexible probes.

4. Exemplary microfluidic neural probes

Development of various types of microfluidic neural probes has created many new opportunities. For example, variations of the technology could not only enable simultaneous drug delivery, optical stimulation, and electrophysiological recording but also delivery of pharmacological agents to multiple sites of the brain in parallel. In the early-stage development of microfluidic neural probe technology, fused-silica capillaries or metal cannula were integrated with the microelectrode to enable electrophysiological recordings with concurrent transcranial fluid delivery.[111] Although easy to use, such metal or glass tubing probes have limited applications due to lack of scalability and difficulty in design variation. Moreover, this cannula approach becomes problematic when trying to add other functional modalities to enable simultaneous readouts of neural activity from the same neurons manipulated by the fluid. The problems occur because of the requirement for delicate assembly and the uncertainty in the relative position between the fluidic outlet and the other modality sites upon integration. In efforts to address these issues, researchers have proposed a wide variety of alternative approaches based on various materials and microfabrication techniques described in previous sections. In the following sections, we introduce exemplary microfabricated fluidic neural probes in the two categories of stiff and flexible probes, based on silicon and polymer MEMS technologies, respectively.

4.1. Stiff microfluidic neural probes based on silicon

Silicon MEMS fabrication techniques have emerged as a powerful approach to construct better microfluidic neural probes with capabilities for various configurations and functionalities. These MEMS fabrication techniques have allowed researchers to design versatile devices, which integrate multiple functional modalities with microfluidics. An exemplary case

of a silicon multifunctional probe involves the monolithic integration of neural recording electrodes with the microfluidic components. Fig. 4A shows this type of multifunctional probe. Here, the microchannel was seamlessly sealed using low-pressure chemical vapour deposition of poly-silicon.[91] This monolithic hybrid silicon probe features recording electrodes to probe electrophysiological activity of neurons at multiple locations (*e.g.* 2–16 electrodes per shank have been demonstrated).[82,91]

Extraction sampling of brain fluids (*e.g.* cerebrospinal fluid)[90,110] is an example of an application enabled by enhanced spatiotemporal resolution of microfabricated fluidic neural interfaces. Previously, the local concentration of neurochemical substances was determined using microdialysis probes (relatively large, 0.2–0.4 mm in diameter) based on a chemical gradient across a semi-permeable membrane, which suffers from poor spatiotemporal resolution. A bulk micromachined fluidic probe was developed by Lee *et al.* (Fig. 4B) for sampling cerebral spinal fluid at 50 nl min^{-1} using one channel while infusing artificial cerebrospinal fluid from the other channel at the same flow rate to avoid pressure changes in the interstitial space.[90] The fractions of collected fluid from the striatum of rats were in turn analyzed by liquid chromatography with mass spectrometry for detection of neurotransmitters and metabolites. Integration of microelectrodes in this platform can make further advances toward concurrent electrophysiological recording and monitoring of neurotransmitter release.

Another major advantage of microfabricated neural probes is that the number of microfluidic channels and the probes

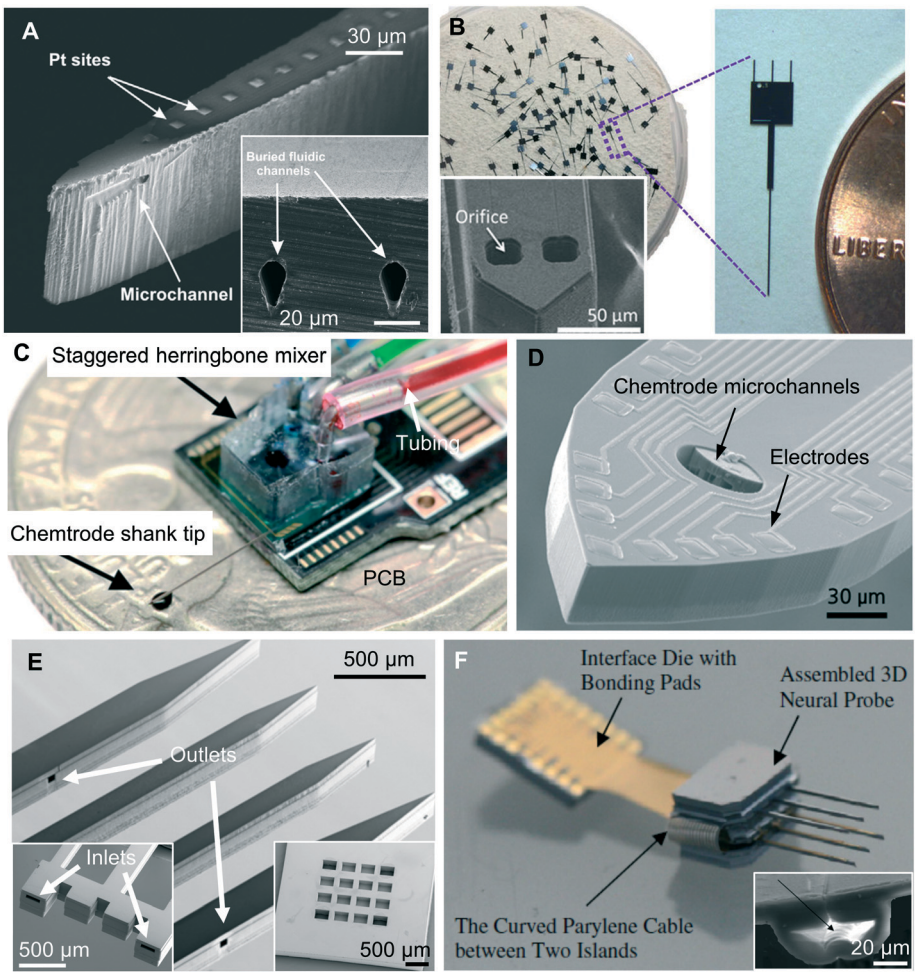

Fig. 4 Stiff microfluidic probes based on silicon. (A) Scanning electron micrographs of a MEMS-fabricated microfluidic neural probe, with monolithic integration of Pt electrical pads.[91] The inset shows the cross-section of the microfluidic channel buried 30 μm below the silicon substrate surface. (B) Photograph of a neural probe capable of sampling brain fluid.[90] The inset shows the scanning electron micrograph of the two orifices at the tip. Photograph (C) and scanning electron micrograph (D) of a multifunctional neural probe with multi-drug delivery capability, which was enabled by integrating a staggered herringbone mixer into a three-inlet PDMS microfluidic chip (C)[81,94] and a silicon multifunctional probe with embedded multiple microchannels (D).[81,82] 3D microfluidic neural probes with two different microfluidic interfaces using a base platform as a frame to hold the 2D array devices (E)[93] and foldable suspended microfluidic cables (F).[87] The insets in (E) show the base of a 2D microfluidic neural probe array (left) and the base platform used to assemble the inlets of the microfluidic probes (right). The inset in (F) shows the scanning electron micrograph of the cross-section of the microfluidic cable (arrow) that interfaces with the assembled 3D neural probe.

themselves can be readily scaled. With the conventional cannula, multiple or repeated fluid administrations are challenging because it requires connection to a different fluid pump or new injection cannulas to be directly inserted into the brain (Fig. 2C). For this reason, repeated administration can increase inflammation as well as physical damage near the ventral tip of the guide cannula. Microfabricated probes can resolve these problems since they can easily integrate multiple microchannels and/or fluidic multiplexers. Fig. 4C shows an example of a multifunctional neural probe with delivery capability of multiple fluids with a fluidic multiplexer.[81,94] Multiplexing the delivery of different fluids without an external manifold was achieved by integrating the silicon microfluidic neural probe with a staggered herringbone mixer in a three-inlet PDMS microfluidic chip. Multiple embedded microchannels in the probe are illustrated in Fig. 4D. This type of multichannel probe enables unique experiments such as examining sequential drug responses, studying the pharmacokinetics of a new drug at different concentrations, or performing localized, *in vivo* immunostaining—all in a single animal.

The scalability of silicon microfabrication extends the dimensionality of the microfluidic probes with multiple shanks. Given the complex structures of the brain, there is an increasing need for 3D arrays of neural probes to cover large areas of the brain. Assembly of 3D microfluidic probe arrays was demonstrated by either inserting microfluidic probes into a base frame platform[93] or stacking 2D probe arrays with spacers between arrays to adjust the distance between probes.[87] Fig. 4E shows an example of a 3D microfluidic neural device assembled by inserting four 2D probe arrays into a base platform. This platform serves as a frame to hold and interface the electrical and fluidic cables with the 2D probe arrays.[93] Here, the fluidic inlets are designed to match the outlets of the base platform for easy assembly and sealing (Fig. 4E, inset). Fig. 4F shows a microfluidic neural device with a 2 × 3 probe array that has been integrated with recording electrodes.[87] In this device, Parylene C was used to seal the XeF_2-etched trenches. The multiple dies of the 2D silicon probe array were also interfaced with Parylene C microfluidic cables (Fig. 4F, inset). Such a simple 3D construction was achieved by folding the Parylene C microfluidic cables, which carry an array of 2D microfluidic probes (Fig. 4F). These 3D microfluidic probes are highly versatile and offer discrete spatial pharmacological intervention across a large area of the brain with a single implant. The minimal tissue displacement by these arrays is unmatched by conventional approaches using multiple cannulas. Overall, scalability and versatility of silicon MEMS techniques hold tremendous potential for creating a wide variety of useful microfluidic tools for *in vivo* neuropharmacology.

4.2. Flexible microfluidic neural probes based on polymers

A primary reason for developing flexible neural probes is to address issues associated with mechanical mismatch between silicon stiffness and soft neural tissues, which have raised questions about the long-term stability of the devices and inflammatory responses. Various polymers have been used to fabricate flexible microprobes for electrical recording of neural activity.[37,38,40] For the same reasons, researchers recently have started to apply the flexible neural interface concept to microfluidic probes. Metz *et al.* (2001) developed one of the first demonstrations of a flexible microfluidic neural probe with recording electrodes made of photopatternable PI using the process described in Fig. 3C-i.[112] The channel layer and the top cover were bonded at 300 °C for 60 min under 300 kPa pressure.[105] Later, the same group modified the device for highly localised delivery of a controlled amount of fluids, suggesting a U-tube shaped channel, which infuses and withdraws the liquid agent at the same time.[105] Fig. 5A shows this device with one fluidic outlet of microchannels and four microelectrodes.[105] The actual performance after being implanted in the brain was not reported.

Another example of a polymer-based neural probe integrated with fluidic channels is an SU-8 based device (Fig. 5B) fabricated using photolithography and thermal bonding (bonding pressure: ~300 kPa; temperature: 100 °C for 20 min; Fig. 3C-i).[67,108] The SU-8 based probe is rigid enough to penetrate an agarose phantom brain as well as rat brain tissue. After insertion of the probe under the dorsal hippocampal sector CA1 (2.2 mm deep), the authors delivered kainate, a glutamate receptor agonist, to induce seizures and observed the typical epileptiform pattern consisting of high amplitude spike and wave rhythmic discharges.[67] Parylene C is another option for flexible neural probes due to its low water absorption rate, chemical inertness, and chronic biocompatibility.[45,50,54] Parylene C microfluidic probes can be fabricated using photoresist-assisted processing (Fig. 3A-i)[106] or thermal bonding (Fig. 3C-ii).[107] Ziegler *et al.* (2006) proposed the design and fabrication of a microfluidic neural probe using Parylene C (Fig. 5C), which enables simultaneous electrophysiological recording and fluid delivery.[107] A deposition-based process for Parylene C could achieve probe thickness smaller than any other devices reported to date (20 μm), which can minimize damage and perturbation to brain tissue. PDMS is also an attractive alternative material for microfluidic neural probes, due to its relatively low elastic modulus (~1 MPa) and optical transparency (>95% transmission in visible wavelengths). PDMS can be moulded by soft lithography followed by oxygen plasma bonding of two PDMS layers to fabricate ultrathin microfluidic devices (Fig. 3C-iii and 5D).[4,14,33] Due to its low modulus of elasticity compared to other polymers (*e.g.* SU-8: 4 GPa,[57–59] PI: 2.5 GPa,[45–49] Parylene C: 2.2 GPa[45,50–52]), PDMS neural implants were shown to be well suited for accommodating physiological movement, as demonstrated in both the brain[14,33] and the spinal cord.[4,113]

These flexible, polymer-based microfluidic neural probes show a relatively low elastic modulus and low bending stiffness, thereby conforming and adapting better to biological tissue than hard materials. However, one limitation of the

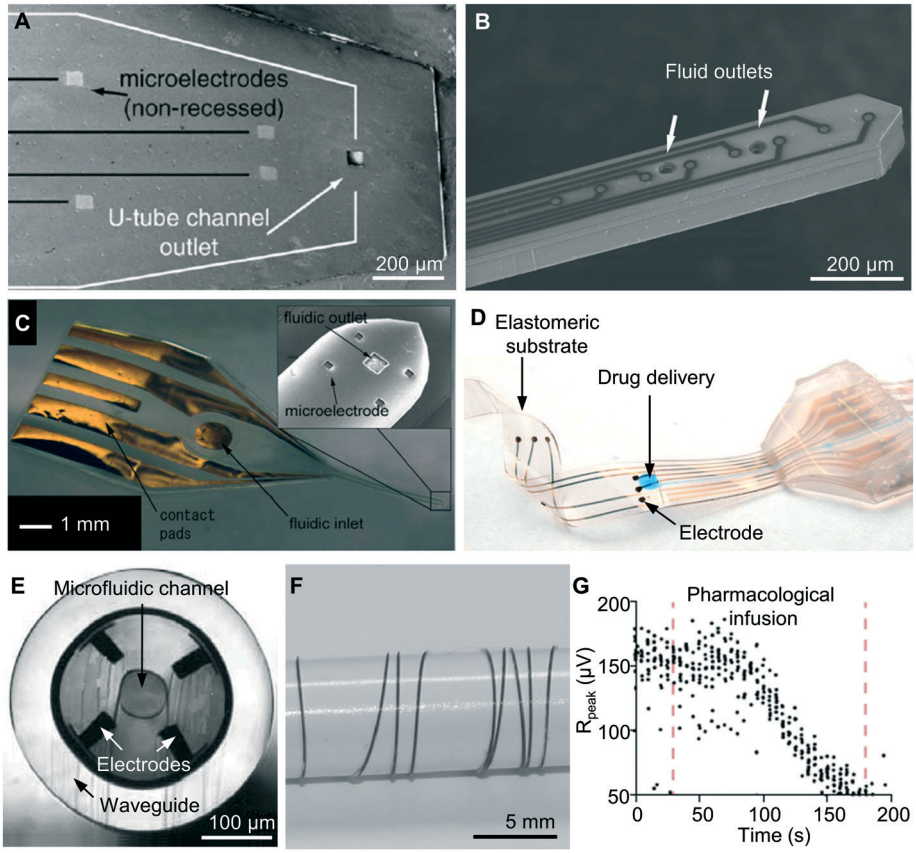

Fig. 5 Flexible microfluidic probes based on polymers. Scanning electron micrographs of the tips of neural probes made with (A) PI[105] and (B) SU-8,[67] and which shows fluid outlets and recording electrodes in close proximity. (C) An optical image of a Parylene C neural probe that captures the overall device structure, including a microprobe, a fluid inlet, and a contact pad for neural signal readout.[107] The inset shows a scanning electron micrograph of the tip of the neural probe with a fluid outlet surrounded by four microelectrodes. (D) A photograph of the electronic dura mater made of PDMS for implantation in the spinal cord.[4] This stretchable neural device is capable of pharmacological delivery and electrical neural stimulation for neuroprosthetics. (E–G) Images and data from a multifunctional fibre system. (E) A scanning electron micrograph of a multifunctional neural fibre that integrates a microfluidic channel, a waveguide, and four recording electrodes.[32] (F) An optical image of a highly flexible multifunctional fibre wrapped around a pencil. (G) Representative electrophysiological data acquired with the fibre showing optically-evoked neural responses during infusion through the same fibre of the AMPA receptor antagonist CNQX to block the evoked effect.

use of ultrathin, soft probes (*e.g.* Parylene C or PDMS probes) is that they do not provide sufficient stiffness to naturally penetrate neural tissue. To overcome this limitation, various strategies have been developed to temporarily stiffen flexible probes to assist implantation. One way is to employ biodissolvable and biocompatible materials, such as polyethylene glycol[106] or maltose.[103] These materials can coat flexible probes or fill microfluidic channels to make probes more rigid for successful injection into neural tissue. Upon injection, the materials are dissolved by biofluids, and the probes accordingly recover their mechanical compliance. Alternatively, an ultrathin injection microneedle can facilitate the implantation process by temporarily mounting it to the flexible probe using silk fibroin.[73,114] Silk fibroin is also a water-soluble, biocompatible material; thus, this approach allows for the release of the injection needle from the flexible probe after implantation. These strategies and other future developments will greatly maximize the utility of flexible microfluidic neural probes.

Many flexible microfluidic platforms based on Parylene C, PI, SU-8, and PDMS (Fig. 5A–D) can be multifunctional by integrating electrodes, optical components, chemical sensors, and more.[4,14,67,104–109] These functional extensions provide various ways to operate the probe, such as co-administration of pharmacological substances and optical stimulation, or simultaneous chemical activation and electrophysiological recordings to investigate neural circuits. However, the manufacturing processes involved in these polymers often require numerous fabrication steps and/or sophisticated assembly processes like transfer printing. These considerations make high yield production of such multifunctional flexible neural probes relatively challenging and create a potential barrier for their commercial translation.

Recent research on manufacturing techniques which mimic the thermal drawing process used to make optical fibres has led to the development of a highly reproducible method for fabricating multifunctional neural probes (Fig. 5E and F).[32,115] The thermal drawing method allows the

integration of multiple materials, including polycarbonate (PC; refractive index, n = 1.58, Young's modulus, E = 2.38 GPa), cyclic olefin copolymer (COC; n = 1.52; E = 3 GPa), and conductive polyethylene (CPE; resistivity, ρ = 30 Ω cm) to create microfluidic channels, waveguides, and electrical probes in a single-fibre platform. Multiple drawing by heating and stretching of a macroscopic template (cm scale in diameter) enables ~200-fold scaling-down of the diameter of multifunctional fibres. This process results in miniature (~400–700 μm in diameter), mechanically compliant (bending stiffness of ~100–150 N m^{-1} in the frequency range of cardiorespiratory activity (0.01–10 Hz) for a 13 mm fibre) neural probes. This approach allows minimally invasive implantation that is suitable for chronic operation in neural tissue. These multifunctional fibres have unique capabilities such as simultaneous pharmacological delivery (infusion rate of 1–100 nl s^{-1}), light delivery (optical loss of 1.6 dB cm^{-1}), and electrophysiological neural recording (contact impedance of 3–5 MΩ at 1 kHz). *In vivo* experimentation shows that this multifunctional neural probe can monitor electrophysiological signals in real time during drug infusion and optogenetic stimulation. Fig. 5G shows that optically-evoked neural responses can be modulated by pharmacological infusion (*i.e.* the AMPA receptor antagonist CNQX (0.1 mM, 2.5 μl) blocks the evoked responses in a Thy1-ChR2-YFP mouse). This novel tool is a powerful option for neural interrogation, which can facilitate long-term *in vivo* pharmacology, electrophysiology, and optogenetics. However, the multifunctional fibre requires highly precise manual microassembly procedures to connect each of micro-scale fluidic channels, optical waveguides, and electrodes to the individual intermediate fluidic, optical, and electrical connectors, respectively, which couple the fibre and external control systems. Therefore, further refinement is necessary to overcome this challenge in the fibre assembly and packaging.

5. Integrated fluid pumps and fluid packaging

A significant bottleneck for implanted microfluidic neural probes in freely behaving animals is the lack of a simple, reliable, and untethered method of fluid infusion. A syringe pump-based system may cause variability in injected volume due to the elasticity inherent to the associated tubing, leading to errors in the intracranial infusion volume (typical <1 μl).[116,117] Additionally, replacing the microsyringe, fluid swivel, or tubing can increase the risk of infection.[118] To overcome these limitations, miniaturized microfluidic systems can be used to integrate active pumps and other fluid packaging components with fluidic neural interfaces. Most previous implants developed for fluid delivery have demonstrated applications in biological organs other than the brain. Although their bulky sizes are not suitable for implantation in the brain, these integrated pumps and fluidic packaging concepts can be adapted for miniaturized microfluidic neural probe systems. Here, we discuss general strategies to miniaturize fluid delivery systems for fully self-contained implants and illustrate several candidates and example applications in neural systems.

5.1. Integrated fluid pumps

An essential component for a fully integrated microfluidic neural interface is a fluid pump for infusing fluid agents through a microfluidic probe. An advanced MEMS technology has been used to miniaturize fluid pumps controlling fluid delivery. Ideal fluid pumps should be able to precisely control flow rate and infusion volume and should have low power consumption, minimum backflow pressure, and biologically-safe actuation.[119] The micropumps can be broadly classified by the principle of actuation into mechanical and non-mechanical pumps.[120] Mechanical pumps account for the pumping systems with mechanically moving parts such as pumping diaphragms, physical actuators, and check valves. Non-mechanical pumps work without any moving parts and can potentially extend the lifetime of devices. Here, we focus on only mechanical pumps because non-mechanical pumps cannot provide temporal control of fluid delivery, which is essential for manipulation of neural circuits. For broader and exhaustive reviews on micropump technologies for self-contained drug delivery devices, see ref. 119–123.

The most popular type of mechanical micropump is a displacement pump, which ejects fluid in a pump chamber by direct pushing with a flexible diaphragm controlled by an actuator.[120] The actuation mechanism of displacement pumps can be classified by electromechanical, thermal, and electrochemical methods as described below. The electromechanical pump directly converts the electrical potential to mechanical forces to push fluid out. This approach can be achieved using electrostatic, piezoelectric, or electromagnetic actuation. Electrostatic actuation uses Coulomb attraction between oppositely charged plates, and piezoelectric actuation makes use of the strain induced by an applied electric field on the piezoelectric crystal. These two methods offer low power consumption and fast response but have limitations in actuation displacements. Electromagnetic actuation is another option for mechanical pumping to displace the diaphragm, which uses an electromagnetic coil and a permanent magnet to generate Lorentz force by currents in energized coils in a magnetic field. Although the electromagnetic actuator consumes a relatively large amount of power, it provides a large displacement and is readily available as a commercial off-the-shelf part with low costs. Fig. 6A illustrates a head-mounted drug delivery device designed for applications in guinea pigs, integrated with electromagnetic actuators as a reciprocating pump for drug infusion and a commercial piezoelectric pump for drug loading to the chamber.[124] This device was designed to infuse and withdraw fluid agents into the cochlea using a pump built with a polyimide diaphragm, a displacement chamber, and a commercial electromagnetic microactuator (11 mm × 13 mm in size). Drugs were loaded into the infusion line using a commercial piezoelectric

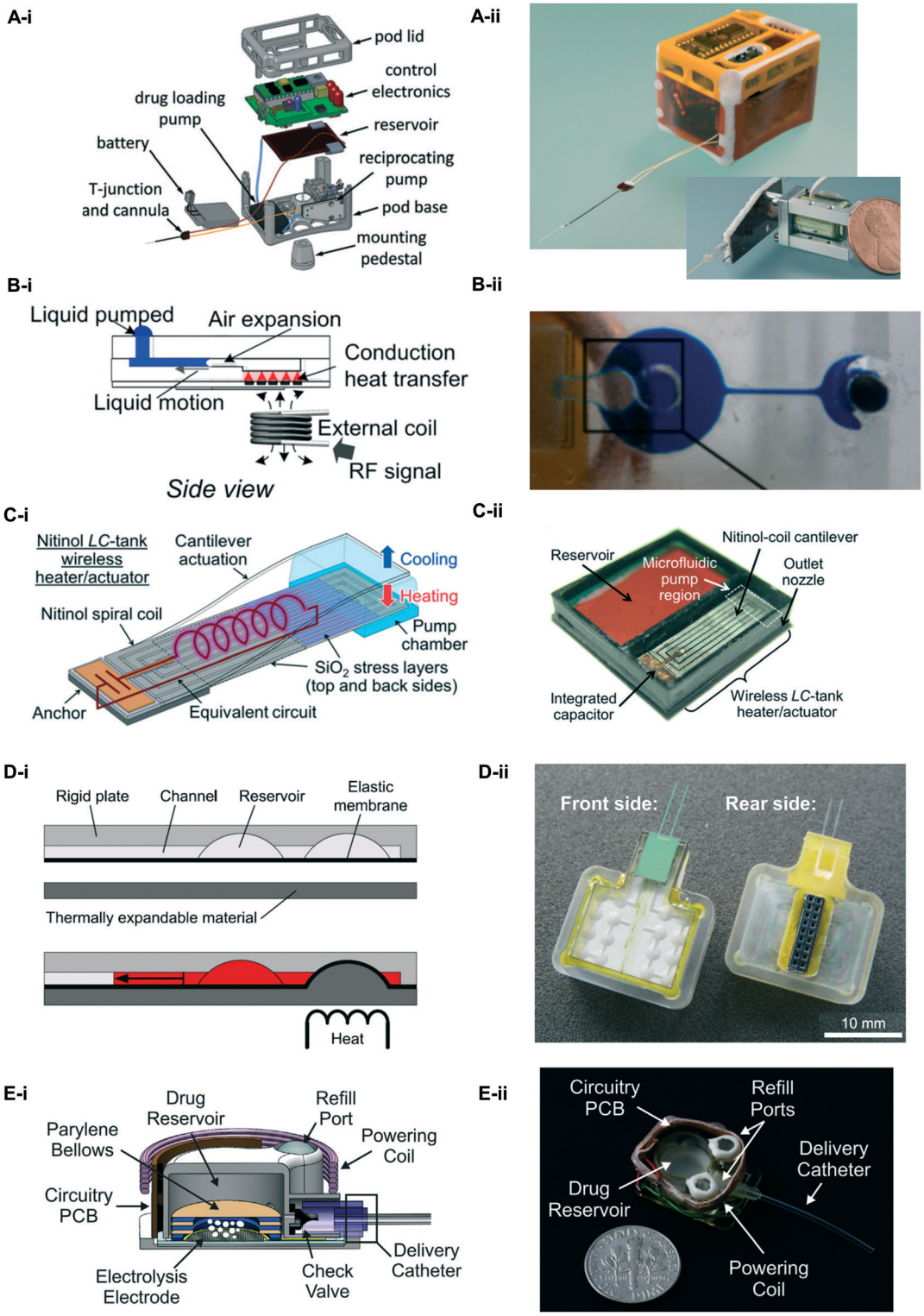

Fig. 6 Miniaturized active pumps for integrated microfluidic implants. (A–E) Images of the integrated micropumps for implanted fluid delivery. (A) A head-mounted drug delivery device integrated with electromagnetic actuators as a reciprocating pump for drug infusion and a commercial piezoelectric pump for loading drugs into the chamber.[124] (A-i) Exploded drawing of the device assembly and (A-ii) photograph of the assembled system. The inset shows the reciprocating flow pump with a miniature electromechanical actuator prior to the final assembly. (B) A thermopneumatic micropump operated by a wireless powered induction heater.[132] (B-i) Illustration of the working principle of the thermopneumatic operation and (B-ii) photograph of the micropump. (C) An implantable drug delivery device employing shape memory alloy pumps.[133] (C-i) Conceptual diagram of the wireless pump and (C-ii) photograph of the RF powered, implantable pump without the top cover. (D) A microfluidic neural probe integrated with active pumps based on a thermally expandable polymer.[142] (D-i) Diagram of the actuation principle of the thermally actuated micropump and (D-ii) photograph showing the front and the rear side of the assembled devices. (E) A drug delivery device using electrolysis-based pumping.[145] (E-i) Schematic diagram showing the architecture of the drug delivery system and (E-ii) photograph of the assembled device.

micropump (30 × 15 × 3.8 mm in size). The final system dimensions and weight were 56.3 × 41.3 × 36.6 mm^3 and 50 g, and the energy consumption per pump cycle was 20.9 J (19.3 J for electromagnetic actuation, 0.958 J for piezoelectric actuation, and 0.717 J for the other electronics). The device could be operated for 50 hours with one battery change. The mean infusion volume was 1.048 ± 0.031 μl with a peak flow rate of 8.064 ± 0.298 μl min^{-1}.

Thermally actuated micropumps are attractive due to their large volume of displacement. In thermally actuated micropumps, an electrical heater is used to raise the local temperature and covert thermal energy into high pressure to displace a diaphragm. However, thermally actuated micropumps can suffer from high power consumption with a relatively slow response.[119] Additionally, care must be taken to isolate heat from fluid agents and biological tissue. Thermopneumatic,[125–132] shape memory alloy,[133–138] and thermally expandable polymers[118,139–142] are popular options for thermally actuated micropumps. In thermopneumatic micropumps, an actuation chamber is filled with a gas or liquid which is expanded and compressed periodically by a heater and a cooler, respectively. This periodic change in volume actuates the membrane with a displacing movement for pumping fluid. Fig. 6B shows an example of a thermopneumatic micropump device operated by a wirelessly powered induction heater.[132] The authors integrated a thermopneumatic micropump with a wireless microheater powered by a planar inductor–capacitor resonator. Frequency tuning of the external magnetic field using an inductive coil transmitter controlled this planar LC heater. The micropump device was able to deliver a minimum volume of 96 nl at a temperature of 29 °C (4 °C elevated from 25 °C) after being thermally activated for 10 s. The fluid volume dispensed from the micropump was linearly controlled from 17 nl s^{-1} to 88 nl s^{-1} by increasing the joule heating power from 0.07 W to 0.89 W. The final dimensions of the thermo-pneumatic micropump were 22 × 7 × 4 mm^3. Its potential for further miniaturization makes this type of pump an attractive option for a self-contained microfluidic system for the brain. Shape memory alloy and bimetallic micropumps are based on the shape memory effect of special alloys (*e.g.* titanium nickel) and the difference in thermal expansion coefficients of materials, respectively. Both actuation mechanisms require a high power (typically >100 mW) but can generate a large force when heated. Fig. 6C shows an example of an implantable drug delivery device employing shape memory alloy pumps.[133] The device was packaged by PI with dimensions of 10 × 10 × 2 mm^3, which contained a micromachined pump chamber and Parylene C check valves. The micropump was validated to repeatedly dispense a single release volume of 219 nl from a reservoir of 76 μl when wirelessly powered by RF fields with an output power of 1.1 W.

An actuator based on thermally expandable polymers can facilitate the construction of miniaturized, lightweight integrated pumps as demonstrated for microfluidic neural interfaces for the brain.[14,118,142] Fig. 6D shows a microfluidic neural probe integrated with this type of pump, which was developed by Spieth *et al.* (2012).[118,142] The device was built by mounting hemispherical reservoirs on a thermally expandable polymer layer, layered on top of an array of microheaters. The thermally expandable polymer composite was made by mixing PDMS with thermally expandable microspheres, called Expancel®, which contain a small amount of liquid hydrocarbon in a gas-tight thermoplastic shell.[139,141] Upon heating above a critical temperature (76–81 °C), the polymeric shell softens and the liquid hydrocarbon undergoes a phase change to gas, resulting in the volumetric expansion of the expandable layer by a factor of up to 60.[118] This volumetric expansion is irreversible, thereby preventing backflow of ejected liquid. Spieth *et al.* demonstrated the device for the brain implant with the final dimensions of 11 × 15 × 3 mm^3 [118] or 20 × 17.5 × 5 mm^3,[142] which contains 16 reservoirs each having a capacity of 0.25 μl and a power consumption of 225 mW over 15 s. The reduced complexity of the microfluidic interfaces of such micropumps has opened up the opportunity for stand-alone operation as well as wireless controllability.[14]

Electrochemical actuation is another compelling option for miniaturized microfluidic neural interfaces. Electrochemical pumps use electrolysis to dissociate water into oxygen and hydrogen, creating gas bubbles that provide the driving force to dispense liquids.[143] The electrochemical micropump requires relatively simple fabrication techniques and consumes relatively low power (on the order of μW–mW).[144] Early approaches to miniaturize fluidic delivery systems for the brain were demonstrated by this electrochemical actuation.[116,117] However, direct electrolysis of drug solution to generate the infusion pressure has a risk of degrading drug quality. Recent development bypassed this potential problem by making an electrochemical micropump that separates the drug solution and water required for electrolysis. This device was constructed with a pair of interdigitated platinum electrodes and an electrolyte (*e.g.* water) sealed with expandable Parylene bellows (Fig. 6E).[145,146] With electrolysis activation, the bellows expand and can subsequently pump out the drug solution from the reservoir. This device presented by Cobo *et al.* (2016) was designed for wireless infusion of pharmacological agents (*e.g.* anti-cancer drug and siRNA-gold nanorod) into xenograft tumors in nude mice. It has dimensions of 20 × 15 × 8.1 mm^3 and weighs 4.1 g.[145] The reliability and reusability of this electrochemical pump make it attractive for long-term applications. An *in vivo* study showed that the device could reliably deliver daily doses of 30 μl in a freely moving rodent for three weeks with less than 6% variation in flow rate. Further miniaturization and optimization of these mechanical pumps will greatly facilitate integration of fluid pumps to enable entirely self-contained microfluidic neural probe systems toward untethered operation.

5.2. Fluid packaging

Proper fluid packaging is necessary to prevent undesired fluid leakage and evaporation from reservoirs in any variety of microfluidic neural probe systems. *In vivo* fluid administration enables many options for neural circuit manipulation and disease treatment by delivering controlled amounts of pharmacological agents to specific areas of the central and

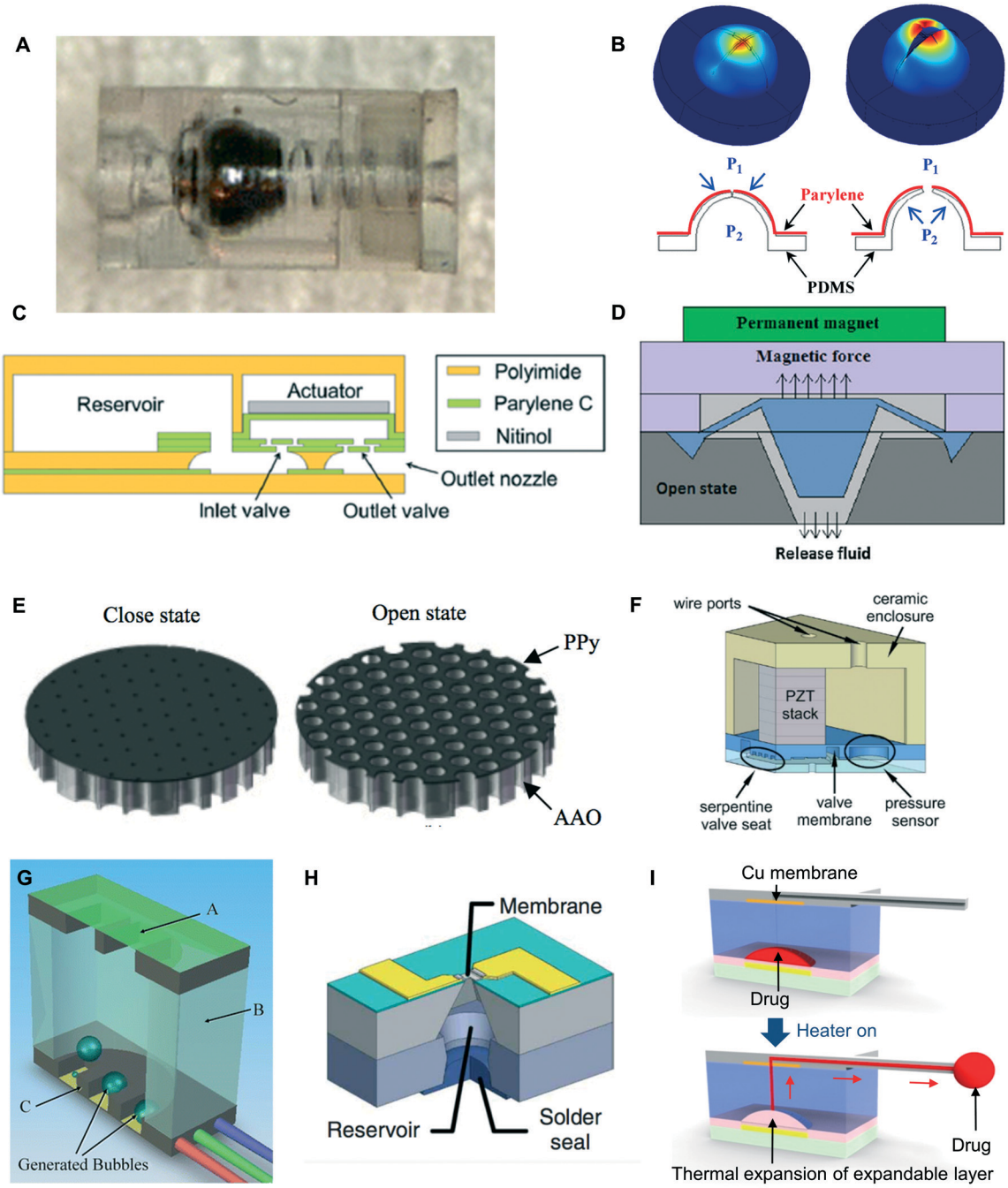

Fig. 7 Strategies for controlled drug release to prevent fluid leakage. (A) An in-plane ball-and-spring check valve designed to be sealed with heat shrink tubing.[146,147] (B) Hemispherical parylene/PDMS microvalves designed for controlled fluid release.[148] (C) Parylene C valves/polyimide reservoir actuated by magnetic induction heating of a nitinol membrane.[133] (D) A magnetically actuated microvalve with an iron-doped PDMS plug and a Si/PDMS chamber.[150] (E) An array of electrically actuated polypyrrole nanovalves on an anodized aluminum substrate.[151] (F) Cross-section of a microvalve actuated with lead zirconate titanate (PZT), a piezoelectric material, with an integrated pressure sensor to enable dynamic flow rate control.[156] (G) A hermetically sealed chamber with a silicon nitride membrane, ruptured by bubbles generated by resistive heating.[167] (H) A polyethylene glycol reservoir hermetically sealed with a bead of indium-tin solder and a membrane made either of gold or of multiple layers of titanium and platinum.[163,164] (I) A hermetically sealed chamber with a copper membrane, ruptured by increasing pressure *via* thermal expansion of an expandable polymer layer on the bottom of the chamber.[14]

peripheral nervous systems. However, misadministration of pharmacological fluids in the wrong dosage can lead to unwanted neural modulation or serious physiological consequences. In addition, it is important that fluids be preserved in reservoirs for long-term experimental or treatment options to be efficacious. Careful fluid packaging strategies can mitigate the risks of these concerns. To prevent misadministration of fluids, schemes for both fluid leakage and fluid evaporation must be considered in the device design.

5.2.1. Check valves for leakage prevention. One way to prevent undesired fluid release is by integrating mechanical valves into the fluid delivery systems. This approach is advantageous because it can create a reusable device with a refillable reservoir for multiple fluid deliveries over time. The simplest type of valve for microfluidic applications is the check valve, a valve that opens with a pressure gradient in one direction but closes with a pressure gradient in the opposite direction. Check valves have the significant advantage of requiring no actuators, making them easy to fabricate and implement. Fig. 7A shows one type of check valve with a spring, designed to be sealed in heat-shrink tubing.[146,147] If pressure within the tube is raised above a certain threshold relative to the pressure outside the tube, the spring force is overcome and fluid will be able to flow out. However, the valve will resist a very large exterior pressure relative to the pressure inside the tube, shutting the valve firmly. The same capability can be achieved by constructing hemispherical check valves using Parylene C/PDMS as shown in Fig. 7B.[148] This design attempts to mimic the functionality of naturally present arachnoid granulations in the brain and takes inspiration from the one-way PDMS valves commonly found in condiment bottles. The hemispherical PDMS valve structure facilitates effective sealing, while Parylene C coated on the PDMS valve prevents fluid from diffusing through the valve material.[148] Fig. 7C shows another example of a check valve integrated into a fluid pumping device.[133] In this device, as the nitinol (nickel–titanium shape memory alloy)-based actuator changes its shape (bent either inside or outside) in the presence of an external magnetic field, it sequentially opens and closes the inlet and outlet valves to pump out fluid from the reservoir (nitinol actuator bent inside – inlet valve closed and outlet valve open; actuator bent outside – inlet valve open and outlet valve closed).[133] Although effective, this design (10 mm × 10 mm × 3 mm) has large space requirements for the reservoirs and pumping modules, which may limit the scaling potential of the overall system for implantation in small animals such as mice and rats.

Actively actuated microvalves are another option for controlling fluid flow and preventing unnecessary fluid leakage. One example is a magnetically actuated microvalve (Fig. 7D).[149,150] This design involves a valve plug made of PDMS doped 50% by weight with iron particles (<10 μm in size).[149] An external magnetic field can be applied to actuate the valve and release a specified fluid volume. The device could be implanted subdermally and actuated by holding a permanent magnet on the surface of the skin. This is a simple design, but the need for an external permanent magnet in close proximity to the device for actuation can make the system unsuitable for use in actively moving animals such as mice and rats. More compact designs can be achieved using shape-tunable materials such as polypyrrole (PPy)[151–154] and piezoelectric materials.[155–157] PPy microvalves built on an anodized aluminium oxide (AAO) substrate can open or close with an applied voltage when aqueous sodium ions are present (Fig. 7E).[151] Similarly, a piezoelectrically actuated valve can actively modulate fluid delivery with voltage control (Fig. 7F).[155–157] Combined with a pressure sensor for feedback control, this device not only prevents undesired fluid leakage but also precisely controls the flow rate of fluid delivery.

Hermetically sealed reservoirs with thin metal membranes also provide effective and complete prevention against fluid leakage. Although this type of reservoir is only able to dispense one particular, pre-determined fluid volume exactly once, this simple design facilitates integration of separately fabricated microfluidic probes for fluid delivery deep into the brain. The fluid is released when a membrane forming one wall of the reservoir is punctured. Thin metal membranes (*e.g.* gold,[158–162] platinum,[163,164] or copper[14]) can seal the fluid outlet port by physical vapour deposition or transfer printing. These membranes are on the order of 300 nm–3 μm and can be punctured by expanding gases generated either in electrolytic processes[165,166] or *via* resistive heating[167] (Fig. 7G). Alternatively, thin metal membranes that seal reservoirs can be ruptured by electrochemical dissolution,[158,160–162] by joule heating from a supplied current (Fig. 7H),[163,164] or by increasing fluid pressure through volumetric expansion of a thermally expandable polymer in the reservoir (Fig. 7I).[14] The first approach is effective only when the gold membrane cap is in contact with saline, whereas the other two actuation mechanisms are environmentally-independent, making them more useful for a wide variety of scenarios. Researchers also demonstrated the scheduled and controlled release of drugs from reservoirs sealed with bio-degradable polymer membranes (poly(lactic-co-glycolic acid)), which could be tuned to degrade after differing amounts of time *in vivo*.[168] Unfortunately, this type of device cannot provide temporal control of fluid delivery and is therefore inappropriate for applications requiring manipulation of neuronal activities with high temporal resolution. Depending on target applications, careful consideration should be made to determine an optimal fluid packaging strategy from the available toolset.

5.2.2. Device packaging for fluid evaporation prevention. Fluid evaporation from a reservoir can be avoided largely through careful material selection for device packaging. Any material used to form a reservoir must be impermeable to the contained fluid or fluid vapour; otherwise, fluid

evaporation will occur through the reservoir walls. Multiple materials with uniform crystal structures (*e.g.* silicon,[169,170] silicon nitride,[171] glass,[167] metals[14,158–164]) have shown negligible water vapour penetration, and some polymers (*e.g.* cyclic olefin polymer (COP),[14] Parylene C[14,148,172]) have been demonstrated to store fluids for long time by minimizing evaporation. Reservoirs made of gas permeable materials (*e.g.* PDMS) can also be effective for long-term storage of fluids when coated with a highly impermeable polymer such as Parylene C.[14,148,172] Table 1 shows the water vapour permeability of various polymers that can be used to construct fluid reservoirs.

6. Toward wireless *in vivo* microfluidics

Advances in materials and manufacturing approaches for microfluidic neural probes have enabled minimally invasive, localized pharmacological intervention for dissecting neural circuits, molecular pathways, and cellular signalling. However, the majority of drug infusion studies for neural circuit manipulation use syringes coupled to external pumps *via* polyethylene tubing connected to the neural probe implanted within the brain region of interest (Fig. 2). While relatively easy for most labs to implement, these tethered approaches severely limit the animal's behaviour. In particular, experiments involving social behaviour, aggression, and related complex naturalistic behaviours are difficult to achieve in a tethered scenario. Furthermore, these tethered implants potentially increase neural tissue damage in the brain region of interest due to repeated entry of the internal cannula into the brain tissue and subtle movement associated with small forces exerted by the tethered and skull-mounted materials. Such implant- and tether-related micromotions have recently been directly observed through deep brain microendoscopy.[173] This damage can prevent appropriate interfacing with the relevant biological modalities in the brain. For this reason, there is an urgent need for wireless *in vivo* microfluidics.

6.1. Wireless control and power harvesting technologies

Integration with wireless technologies, such as radio frequency (RF)[9,73,113,114,174–181] and infrared (IR),[14,182,183] has successfully enabled wireless electrophysiological neural stimulation and recording as well as wireless optogenetics. RF technology can be engineered to provide both wireless power transfer and bidirectional data communication, while the IR approach uses a separate power source (*i.e.* batteries) for one-way data transfer from the remote controller to the receiver module mounted on the animal. Both IR and RF technologies are suitable for enabling wireless fluid delivery, as both types of signals can trigger the wireless modules to turn on the integrated fluid pumping systems for drug delivery. The following sections and Table 3 describe IR and RF wireless technologies that can be potentially applied to enable wireless control of *in vivo* microfluidics as well as other types of neural implants.

6.1.1. IR controlled wireless technology. IR light is widely used for short-range (1–10 m) remote controls. For wireless control, the IR transmitter (*e.g.* IR light-emitting diodes) sends data bits as a series of light pulses with wavelengths typically in the 940–950 nm range to the receiver (*e.g.* a photodetector). Low cost construction and simple implementation can provide independent control over multiple channels.[14,183] These features make them suitable for remote control of neural probes by triggering electrical, optical, and/or chemical stimulation.[14,182,183] However, the utility of IR is limited by a number of factors such as an inherent 'line of sight' handicap and a need for a power supply such as batteries.

6.1.2. RF wireless technology. RF remote control and powering systems use radio signals ranging from 3 kHz to 300 GHz. Their operation critically relies on the extent to which an operating frequency of a transmitter is matched to that of the receiver as it establishes a successful

Table 3 Overview of various wireless technologies used for neural implants[184,186]

		RF wireless data communication			RF wireless power harvesting	
Wireless technology	Infrared	Bluetooth	Zigbee	WiFi (802.11x)	High frequency inductive coupling	Ultra-high frequency RF coupling
Frequency	940–950 nm (signal)/a few tens of kHz (carrier)	2.4 GHz	868/915 MHz or 2.4 GHz	2.4–5.8 GHz	1–2 MHz/13.56 MHz (ref. 176 and 188–193)	On the order of GHz (ref. 9, 113 and 200)
Range	Up to 10 m	10–100 m	70–300 m	100 m	A few centimeters[a]	<20 cm[a]
Data rate	0.5–1 kbps	Up to 1 Mbps	20 kbps/40 kbps or 250 kbps	11–200 Mbps	N/A	N/A
Power consumption/delivery	20–200 mW	10–500 mW	30 mW	750–2000 mW	10 mW	10 mW
Battery requirement	Yes	Yes	Yes	Yes	No	No
Data transfer	Uni-directional	Bi-directional	Bi-directional	Bi-directional	Uni-directional	Uni-directional

[a] The distance from the source coil antenna.

communication. The following sections highlight two major lines of research: wireless data transmission and radio frequency wireless power harvesting.

6.1.2.1. RF wireless data transmission technology

i. Bluetooth. Bluetooth is a short range wireless communication technology that operates in the 2.4–2.4835 GHz ISM (Industrial, Scientific, and Medical) band (IEEE 802.15.1).[184] This technology offers several advantages including a large enough range of operation (10–100 m) to cover various behavioural neuroscience experiments in the lab, no 'line of sight' handicap, and easy integration with PCs or smartphones. A few neural recording systems have been successfully implemented utilizing Bluetooth technology with batteries[185] or with inductive power coils.[176] Furthermore, recent advances in BLE (Bluetooth Low Energy) technology have lowered power consumption (peak current consumption <15 mA). This technology enables not only wireless control of neural probes for simultaneous neural stimulation and recording but also manipulation of a specific animal among a group of multiple animals by device pairing. These are powerful features that can empower various behavioural neuroscience experiments.

ii. Zigbee. Similar to Bluetooth, Zigbee provides a low-power wireless communication over short distances (10–100 m) but is more suitable for control of multiple devices in a network. ZigBee uses the 2.4 GHz ISM band (IEEE 802.15.4) and runs on a mesh topology network where data from a node travels through a network of nodes until it reaches the destination.[186] This technology offers several advantages such as a lower module price than Bluetooth and Wi-Fi, lower power consumption than Bluetooth, easier Internet integration, and capabilities for bi-directional communication and quasi-simultaneous control of multiple devices in a network. Researchers have demonstrated wireless neural devices using MiWi[175] (simple version of Zigbee) and Zigbee[187] protocols for neural stimulation applications.

iii. Wi-Fi. Wi-Fi is a wireless networking technology that connects devices with each other and to the Internet (IEEE 802.11x) using the 2.4 GHz radio band for 802.11b, 802.11g, or 802.11n and the 5 GHz band for 802.11a.[184] Its main advantage lies in applications involving high wireless data throughput and its easy integration to the Internet for control of neural devices at remote sites, without any directional line of sight requirements. Although Wi-Fi consumes relatively high power for its operation, integrating this technology with other low power protocols (*i.e.* Bluetooth or Zigbee) can open avenues for energy-efficient Internet control of interconnected neural probe systems, which can possibly lead to high throughput neuroscience experiments at a remote site.

6.1.2.2. RF wireless power harvesting/control technologies

i. High frequency range (3 kHz–300 MHz) inductive/magnetic resonant coupling. Inductive coupling between a source coil and a load coil occurs when the source coil (transmitter) induces an alternating voltage across the load coil (receiver), leading to energy transfer. Although this experimental approach has some utility,[176,188–193] a small range of operation (a few centimeters) and low power transfer efficiency of inductive coupling limit its practical application because reducing the size of the receiver coil degrades its effectiveness. The magnetic resonant coupling can be an attractive alternative. In high frequency inductive coupling, typically a source or load coil includes resistance and limits quality factor to modest values. As a result, a two-coil system achieves low transmission efficiency.[176,188–193] However, a three- or four-coil system where a primary coil and a secondary coil consisting of purely reactive components such as capacitors and inductors are added to the two-coil system can achieve high transmission efficiency (>80%) over a two-coil system.[194–198] Such magnetic resonant coupling allows power transmission only when the resonant frequency of the load coil matches that of the source or primary coil, thereby minimizing the sensitivity of the system to electrical noise in the surroundings for robust, reliable operation. A recent work by Shin *et al.* (2017) demonstrated near-field wireless power transfer for optogenetic behaviour control by using RF transmission loop antennas surrounding an animal enclosure.[181] Inductively coupled antennas, which operate at 13.56 MHz, could harvest sufficiently high, uniform power for optoelectronic implants in a cage (30 cm × 30 cm × 15 cm) surrounded by a dual-loop antenna.

ii. Ultra-high frequency (UHF) range (300 MHz–300 GHz) RF coupling. The major disadvantage of the high frequency range inductive/magnetic resonant coupling is its form factor that makes them less ideal for small animal studies. When dimensions of coil systems operating at high frequency ranges are scaled down to 1 cm, transmission efficiency drops to extremely low values.[199] Systems operating at 'ultra-high' frequency ranges can achieve highly efficient systems at a given dimension below 1 cm. Recent studies demonstrated that ultra-miniaturized RF power harvesting/control systems can provide a unique, biocompatible platform for wireless delivery of light to any part of the body in a freely behaving animal.[9,113,200] One issue on ultra-high frequency electromagnetic wave propagation is attenuation of electromagnetic waves or absorption of waves into biological tissues when traveling through the tissues. The absorption leads to tissue heating and as a result damages the tissues. IEEE and FCC suggest guidelines to minimize exposures to UHF waves.[201] In addition, these UHF systems are susceptible to changes in angles or orientations of implanted devices. Therefore, careful manipulation of this technology is needed when designing an effective neural implant.

Straightforward extension of this technology would enable wireless *in vivo* microfluidic drug delivery in the central and peripheral nervous systems of freely moving animals.

6.2. State-of-the art wireless microfluidic neural probe systems

A wide variety of wireless neural devices can be implemented using readily available wireless technologies

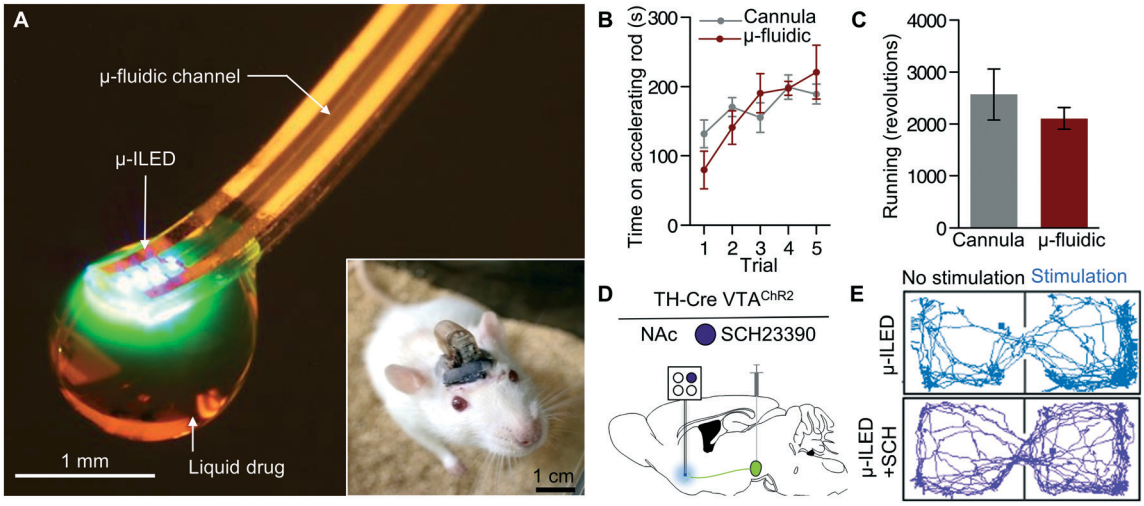

Fig. 8 Wireless microfluidic neural probe for *in vivo* pharmacology and optogenetics. (A) An optical image of the flexible optofluidic probe consisting of multiple microfluidic channels and μ-ILEDs, capable of simultaneous pharmacological delivery and optical stimulation. The inset shows a small (15 × 15 × 7 mm^3), lightweight (1.8 g), wireless optofluidic system implanted in the brain and mounted on the head of a freely moving rat. (B & C) Activity profiles of mice implanted with wireless- and cannula-based devices.[14] (B) Rotarod data showing the equal ability of the animals on the rotating rod as the trial speed increases. (C) Spontaneous locomotor activity on a running wheel is not altered by the wireless optofluidic system. (D) A schematic diagram illustrating the wireless optofluidic experiment. Infusion of channelrhodopsin-2 fused with eYFP was made into the ventral tegmental area (VTA), followed by implantation of an optofluidic device filled with SCH23390 in the nucleus accumbens of tyrosine hydroxylase (TH)-Cre mice 6 weeks later. (E) Traces of mice during real-time place preference control using wireless optofluidics. Optogenetic activation of VTA dopaminergic neurons drives a strong place preference (top), while delivery of SCH23390 (dopamine receptor-1 antagonist) blocks preference behaviour (bottom).

described in the previous section. Wireless drug delivery systems have been demonstrated for various applications,[133,146,202–205] but most of them are not appropriate for neurophysiological applications in small mammals (*e.g.* mice, rats, *etc.*) due to their relatively large physical footprints, insufficiently light weights, and inability to deliver fluids deep into the brain.

A recent innovation from our groups of materials engineers and neuroscientists addressed this issue by developing what is referred to as a wireless optofluidic system – a small, lightweight wireless microfluidic neural probe system that incorporates optoelectronics for *in vivo* pharmacology and optogenetics (Fig. 8A).[14,24] This entirely self-contained, head-mounted system includes an ultrathin flexible microfluidic probe (~50 μm in thickness; stiffness 13–18 N m^{-1}; modulus of elasticity ~1 MPa), microscale inorganic LEDs (μ-ILEDs; dimensions: 100 μm × 100 μm × 6.45 μm), compact thermally actuated fluid pumps, an IR-based wireless control module, and small lithium-ion batteries. This system allows untethered, programmable spatiotemporal control of fluid delivery and optical stimulation deep in the brain. This approach to manipulating neural circuits holds much potential for many neuroscience and clinical applications involving freely moving subjects. The IR wireless control module interfaces with the optofluidic neural probe system to enable streamlined operation of the fully self-contained device. The fully-assembled device weighs only ~1.8 g; therefore, it does not disturb the movement or behaviour of animals. No gross differences in motor function and physical activity were found between optofluidic device-implanted mice and cannulated mice using the rotarod and running wheel tests (Fig. 8B and C). One of the most advanced features of the wireless optofluidic system is its ability to simultaneously implement wireless *in vivo* optical stimulation (*e.g.* for optogenetics) and pharmacology. In a demonstration experiment (Fig. 8D and E), optical stimulation of ventral tegmental area dopaminergic neurons was able to drive a real-time place preference (demonstrating the reinforcing nature of this photostimulation) while concurrent wireless delivery of a dopamine receptor-1 antagonist (SCH23390) blocked this behaviour. Such wireless design is desirable to enable unprecedented cell-type and receptor-selective circuit manipulation in freely moving animals. These types of technology will empower future research in circuit neuroscience as well as foreshadow applications in clinical medicine using similar designs.

7. Potential issues in long-term applications

For long-term application of microfluidic neural probes, it is important to minimize biofouling and risk of infection, as well as probe clogging. For this reason, a material's property not to induce biofouling and inflammation as well as strategies to prevent microfluidic output ports from clogging should be carefully considered. In the following section, we discuss biofouling and clogging issues associated with chronic implantation of microfluidic neural probes.

7.1. Biofouling

Biofouling can cause problems by accumulating unwanted biological materials on the surfaces of neural implants.[206] These materials are commonly proteins adsorbed by the implant materials, but entire cells or bacteria can also accumulate on implant surfaces, greatly increasing the risk of infection. This contaminating layer can also provoke an immune response and lead to inflammation[207] or even block microfluidic channels from properly dispensing fluid.[208] This formation of a biofilm made up of proteins, cells, or bacteria on electrophysiological recording electrodes can also significantly degrade signal quality of neural recordings.[209] While the two former components must be met with engineering solutions, bacterial contamination should be addressed by sterilizing the probes in question prior to implantation. Ethanol, ethylene glycol, and autoclaving are all potential solutions to bacterial contamination, but not all may be appropriate for every material selected for probe fabrication.

The adsorption of cells or proteins onto surfaces of implanted neural probes depends on the selected material. Materials such as gold, silicon nitride, silicon dioxide, silicon carbide, and SU-8 have been shown to resist protein adsorption well and elicit a small immune response.[64,209] Notably, both silicon and PDMS have been shown to be significantly more susceptible to biofouling through protein adsorption, leading to an elevated immune response.[64,210] Despite their good resistance to protein adsorption, SU-8 has been shown to delaminate from a silicon substrate after prolonged exposure *in vitro* to a diluted solution of proteins,[64] and silicon dioxide has been shown to corrode after as little as one month in an *in vivo* application, degrading the performance of the implanted device.[211] As such, when selecting materials for long-term implantation, anti-fouling properties must be taken into account.

Although no current schemes exist to completely remove the risks of biofouling, anti-fouling coatings can be designed to resist the growth of protein and biofilm layers on implantable neural probes. Hydrophobic materials such as PDMS readily and irreversibly accept proteins through hydrophobic interactions. As such, to resist biofouling, polymeric coatings should be hydrophilic, should be electrically neutral, and should have hydrogen bond acceptors.[210] In an effort to render it hydrophilic and increase its resistance to protein adsorption, many studies have used coatings with various functional groups – polysaccharide-based coatings,[212] polyhydroxy-polymer based coatings,[213] hydrophilic amide-based coatings,[214] and fluorinated polymer-based coatings[215] have all been shown to improve the anti-fouling properties. Most recently, polyzwitterion-based coatings have been shown to dramatically resist biofouling from protein adsorption, enabling a variety of biological applications in environments where other polymeric coatings would not function properly.[210,216,217] Discovery and application of anti-fouling coatings such as these is an active field of research itself. For further details on anti-fouling coatings, readers can refer to other articles.[64,209,210,218,219]

7.2. Microfluidic channel clogging

Clogging is a potential concern for any microfluidic device, but particularly for those designed to penetrate tissue. In practice, clogging can be caused by either biofouling at the channel outlet or a size mismatch between the microfluidic channel and the contents being expelled. Using anti-fouling coatings as discussed in the previous section can mitigate the former, but care should be taken in both device design and implantation strategy to ensure that channels are not clogged upon insertion into tissue. Careful *post hoc* examination of microfluidic neural probes should be performed to ensure that the implantation approach does not foul the channels. If it appears that the probes clog during insertion, one possible solution would be to backfill the microfluidic channels with an inert fluid (*e.g.* vehicle solution) to help limit such channel infiltration.

Generally speaking, a size mismatch between the microfluidic channel and the contents being expelled is an unlikely result. This type of content-related clogging should not be a major issue for applications in the brain because almost any drug being infused into the brain should be in solution and in low concentrations. Therefore, the size of individual drug particles or crystals should be irrelevant, assuming the microfluidic channel itself is sufficiently hydrophobic to allow passage of the typically aqueous solution used to dissolve the drugs. While some compounds will require polar aprotic solvents to dissolve, direct administration of these into the brain should be limited whenever possible due to the potentially hazardous effects of such solvents.[220] Even the largest known viral particles are well below a micron in diameter,[221] making a viral particle size mismatch with a microfluidic channel highly unlikely. However, despite size not being a critical issue, electrostatic properties of both the channels and the delivered substrate should be considered. The electrostatic properties of charged particles, such as neuropeptides and cell-penetrating peptides,[222,223] should be considered and determined to be compatible with the chosen microfluidic channel design.

One potential problem area for content-related microfluidic neural probe clogging would be in the delivery of whole cells into the brain such as that seen in neural grafting, the process of transplanting neurons derived from stem cells into the brain.[224–226] Here, such cells typically have diameters of 10–30 microns.[227–230] In addition to the potential for size mismatches between cell diameters and microfluidic channels, delivery of whole neuronal cells might also necessitate consideration of additional anti-fouling treatments to accommodate adhesive properties of these neurons.

For instances when channel clogging is an issue, the following considerations should be taken. To prevent any particles from inhibiting fluid flow, the sieving, bridging, and aggregation of particles must be avoided.[231] Sieving occurs

when particles are too large to fit through microfluidic channels and can be prevented by carefully controlling the size of particles or by engineering the size of microfluidic channels according to the size of the particles. Particles will bridge a channel gap when particle concentration in a fluid is sufficiently high that multiple particles get stuck in the middle of a microfluidic channel. This can be avoided by controlling particle concentration and flow rate. Additionally, particles aggregate when they can bind to the channel or reservoir material as well as to each other, successively forming large clumps that can block the microfluidic channel. Aggregation can be prevented by careful selection of reservoir materials, channel materials, and fluid particles to minimize particle–wall and particle–particle interactive forces.[231,232] Bridging and aggregation are possible if the concentration of the drug changes over time due to evaporation, representing another important consideration during fluid packaging as described previously. Therefore, careful design of microfluidic channels and probe materials is necessary to provide successful fluid delivery without clogging issues.

8. Conclusion: challenges and outlook

Innovation in microfluidic neural probes based on new materials, mechanical concepts, and novel manufacturing/integration approaches leads to breakthroughs in neuroscience and medicine. These technologies not only allow for minimally invasive implantation and localized fluid delivery but also facilitate integration with other modalities (*e.g.* electrical, optical, chemical, *etc.*). This multifunctionality is greatly enabled in miniaturized, versatile platforms. More specifically, the latter feature enables compact single platforms that offer diverse combinatorial options for pharmacological infusion, electrophysiological neural stimulation and recording, and optical manipulation of neurons and neural circuits. Together, these features allow for unprecedented studies on the molecular and cellular basis of behaviour, neuronal development and repair, and plasticity in neural systems. Combined with the scalability provided by well-established microfabrication techniques, microfluidics-based approaches create new opportunities for future development and applications. Materials and fabrication methods for the microfluidic neural probes discussed in this article are compatible with many standard semiconductor manufacturing and soft lithography processes. Therefore, they can be readily adapted and applied for mass production of various types of microfluidic probes for widespread use in neuroscience and clinical medicine.

The microfluidic neural probe has evolved toward wireless, flexible platforms to allow natural movement and behaviour while simultaneously minimizing chronic immunoreactive responses in the neural tissue. Although the current state-of-the-art flexible and wireless microfluidics technologies described here have shown promise, further efforts are necessary to improve the ready use of these devices, as illustrated in Fig. 9. For example, it will be critical to develop integrated micro-pumps with negligible heat generation and low-power consumption for future wireless flexible microfluidic neural devices. This feature will mitigate restrictions on temperature-sensitive compounds, which is a potential issue for the thermally-actuated pumps previously employed in wireless optofluidic systems.[14] Electrochemical,[146] shape-memory alloys,[133] near-infrared activation,[203] and

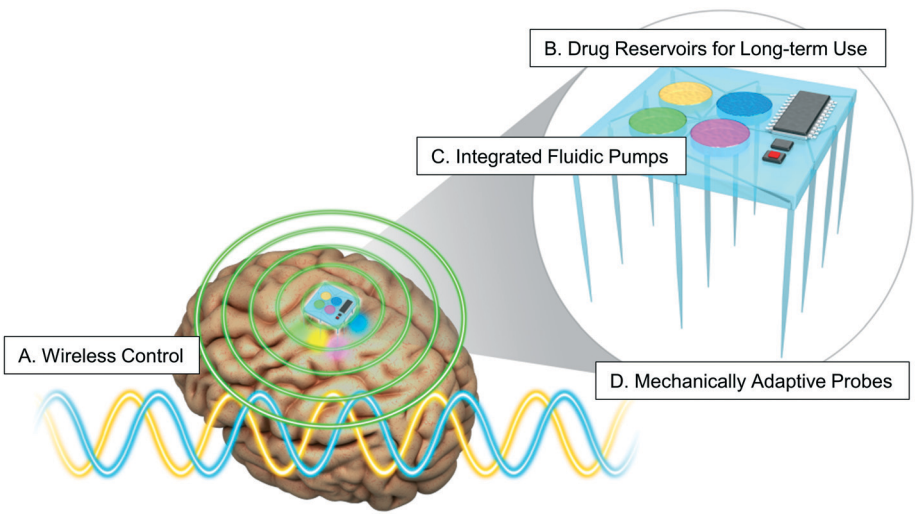

Fig. 9 Vision for future microfluidic neural probe development. Future neuroscience research and clinical applications will be empowered and enriched by developing innovative microfluidic neural probes incorporating the following key designs: (A) wireless technology such as radio frequency-based power and data transfer strategies capable of long-range coverage and simultaneous control of multiple devices. (B) Reusable cartridge-based or refillable drug reservoirs for long-term implantation. (C) Integrated fluidic pumps based on electrochemical actuators, piezoelectric actuators, shape-memory alloys, or other approaches to enable fluid delivery with negligible heat generation and low-power consumption. (D) Mechanically adaptive probes for both simple implantation and long-term mechanical biocompatibility. Such probes may take advantage of shape-memory polymers and alloys, electroactive polymers, low-melting-point alloys, or rigidity tunable composites.

piezoelectric pumps[233,234] are some of the most promising alternatives with demonstrated utility in other drug delivery applications. Another essential aspect of future wireless microfluidic neural probes is the access to greater volumes for long-term pharmacological treatment. One such solution would be the creation of replaceable or refillable cartridge-like reservoirs. This approach would facilitate long-term pharmacological delivery without the need for replacing the entire "used" microfluidic system from the neural tissue *via* disruptive surgery. A system to simply replace or refill the empty reservoirs would keep both the implanted probes and neural tissue intact. Furthermore, innovative wireless technology is desired to provide long-range coverage, simultaneous control of multiple animals, and battery-free operation to enable advanced behavioural neuroscience experiments as well as practical clinical implementation. Among many wireless technologies, the RF wireless approach is one of the most attractive options due to its long-range operation (over 10 m), no 'line of sight' handicap, bi-directional communication capability,[186] and its capability for wireless power transfer.[9,73,113,114,176,235,236] Finally, 'mechanically adaptive' probes (*i.e.* a functional probe that softens upon injection into the neural tissue) would be highly beneficial to address issues with current injection assisting tools[73,114] or biodissolvable polymer approaches.[103,106] Such adaptive neural probes are ideal for both minimizing tissue damage and facilitating the implantation process because they eliminate much of the complexity and cumbersomeness of existing methodologies. Continued investigation on materials featuring a tunable modulus (*e.g.* shape-memory polymers and rigidity tunable composites)[72,237–240] together with engineering efforts to design and manufacture neural probes with those new materials will help accelerate practical applications of this approach.

The neuroscience community is poised to make great, fundamental discoveries in brain function and disease but remains in great need of advanced microfluidic neural probe systems. These devices will need to use biologically and biomechanically compatible materials, be multimodal/multifunctional, and operate by wireless control to engage neuronal function in freely moving animals with high spatiotemporal resolution. Innovative microfluidic interface technologies will establish new horizons for *in vivo* pharmacology, chemogenetics,[22,28,29] optogenetics, and the relatively new field of optopharmacology,[25–27,241–243] which uses light-regulated control of molecules to enable stimulation or inhibition in specific cells with high temporal and spatial precision. Beyond fundamental research, the microfluidic probe approach also has significant potential in clinical medicine, due to its capability of highly localized pharmacological infusion for targeted therapies without affecting neighbouring neural tissues. Such fascinating characteristics will be invaluable for many clinical applications, including treatment of brain tumours, neural injury, and many neurodegenerative diseases (*e.g.* Parkinson's disease, Alzheimer's disease, Creutzfeldt–Jakob disease, *etc.*). Multidisciplinary future development will lead to compelling outlooks in neuroscience and clinical treatment by enabling advanced, multifaceted functions and capabilities that go far beyond what conventional approaches have not been able to conquer.

Acknowledgements

This work was supported by startup funds from the University of Colorado Boulder and Washington University in St. Louis. The images in Fig. 1–2 and 4–8 are reproduced with permission from the references cited in the figure captions.

References

1 T. R. Insel, S. C. Landis and F. S. Collins, *Science*, 2013, **340**, 687–688.
2 A. Schwartz, *Ann. Neurol.*, 2013, **73**, A7.
3 S. Grillner, N. Ip, C. Koch, W. Koroshetz, H. Okano, M. Polachek, M. Poo and T. J. Sejnowski, *Nat. Neurosci.*, 2016, **19**, 1118–1122.
4 I. R. Minev, P. Musienko, A. Hirsch, Q. Barraud, N. Wenger, E. M. Moraud, J. Gandar, M. Capogrosso, T. Milekovic, L. Asboth, R. F. Torres, N. Vachicouras, Q. Liu, N. Pavlova, S. Duis, A. Larmagnac, J. Vörös, S. Micera, Z. Suo, G. Courtine and S. P. Lacour, *Science*, 2015, **347**, 159–163.
5 F. B. Wagner, W. Truccolo, J. Wang and A. V. Nurmikko, *J. Neurophysiol.*, 2015, **113**, 2321–2341.
6 J. T. W. Kuo, B. J. Kim, S. A. Hara, C. D. Lee, C. A. Gutierrez, T. Q. Hoang and E. Meng, *Lab Chip*, 2013, **13**, 554–561.
7 D. P. Hibar, J. L. Stein, M. E. Renteria, A. Arias-Vasquez, S. Desrivières, N. Jahanshad, R. Toro, K. Wittfeld and L. Abramovic, *et al.*, *Nature*, 2015, **520**, 224–229.
8 M. R. Warden, J. A. Cardin and K. Deisseroth, *Annu. Rev. Biomed. Eng.*, 2014, **16**, 103–129.
9 K. L. Montgomery, A. J. Yeh, J. S. Ho, V. Tsao, S. Mohan Iyer, L. Grosenick, E. A. Ferenczi, Y. Tanabe, K. Deisseroth, S. L. Delp and A. S. Y. Poon, *Nat. Methods*, 2015, **12**, 969–974.
10 E. J. O. Hamel, B. F. Grewe, J. G. Parker and M. J. Schnitzer, *Neuron*, 2015, **86**, 140–159.
11 J. H. Jennings, R. L. Ung, S. L. Resendez, A. M. Stamatakis, J. G. Taylor, J. Huang, K. Veleta, P. A. Kantak, M. Aita, K. Shilling-Scrivo, C. Ramakrishnan, K. Deisseroth, S. Otte and G. D. Stuber, *Cell*, 2015, **160**, 516–527.
12 D. J. Chew, L. Zhu, E. Delivopoulos, I. R. Minev, K. M. Musick, C. A. Mosse, M. Craggs, N. Donaldson, S. P. Lacour, S. B. McMahon and J. W. Fawcett, *Sci. Transl. Med.*, 2013, **5**, 210ra155.
13 B. V. Ineichen, L. Schnell, M. Gullo, J. Kaiser, M. P. Schneider, A. C. Mosberger, N. Good, M. Linnebank and M. E. Schwab, *Nat. Protoc.*, 2017, **12**, 104–131.
14 J.-W. Jeong, J. G. McCall, G. Shin, Y. Zhang, R. Al-Hasani, M. Kim, S. Li, J. Y. Sim, K.-I. Jang, Y. Shi, D. Y. Hong, Y. Liu, G. P. Schmitz, L. Xia, Z. He, P. Gamble, W. Z. Ray, Y.

Huang, M. R. Bruchas and J. A. Rogers, *Cell*, 2015, **162**, 662–674.
15 T. E. Anthony, N. Dee, A. Bernard, W. Lerchner, N. Heintz and D. J. Anderson, *Cell*, 2014, **156**, 522–536.
16 D. Rei, X. Mason, J. Seo, J. Gräff, A. Rudenko, J. Wang, R. Rueda, S. Siegert, S. Cho, R. G. Canter, A. E. Mungenast, K. Deisseroth and L.-H. Tsai, *Proc. Natl. Acad. Sci. U. S. A.*, 2015, **112**, 7291–7296.
17 J. H. Jennings, D. R. Sparta, A. M. Stamatakis, R. L. Ung, K. E. Pleil, T. L. Kash and G. D. Stuber, *Nature*, 2013, **496**, 224–228.
18 A. M. Stamatakis, J. H. Jennings, R. L. Ung, G. A. Blair, R. J. Weinberg, R. L. Neve, F. Boyce, J. Mattis, C. Ramakrishnan, K. Deisseroth and G. D. Stuber, *Neuron*, 2013, **80**, 1039–1053.
19 J. J. Walsh, A. K. Friedman, H. Sun, E. A. Heller, S. M. Ku, B. Juarez, V. L. Burnham, M. S. Mazei-Robison, D. Ferguson, S. A. Golden, J. W. Koo, D. Chaudhury, D. J. Christoffel, L. Pomeranz, J. M. Friedman, S. J. Russo, E. J. Nestler and M.-H. Han, *Nat. Neurosci.*, 2014, **17**, 27–29.
20 S. C. P. Williams and K. Deisseroth, *Proc. Natl. Acad. Sci. U. S. A.*, 2013, **110**, 16287.
21 J. G. McCall, R. Al-Hasani, E. R. Siuda, D. Y. Hong, A. J. Norris, C. P. Ford and M. R. Bruchas, *Neuron*, 2015, **87**, 605–620.
22 T. J. Stachniak, A. Ghosh and S. M. Sternson, *Neuron*, 2014, **82**, 797–808.
23 M. Creed, V. J. Pascoli and C. Lüscher, *Science*, 2015, **347**, 659–664.
24 J. G. McCall, R. Qazi, G. Shin, S. Li, M. H. Ikram, K.-I. Jang, Y. Liu, R. Al-Hasani, M. R. Bruchas, J.-W. Jeong and J. A. Rogers, *Nat. Protoc.*, 2017, **12**, 219–237.
25 R. H. Kramer, A. Mourot and H. Adesnik, *Nat. Neurosci.*, 2013, **16**, 816–823.
26 M. R. Banghart and B. L. Sabatini, *Neuron*, 2012, **73**, 249–259.
27 M. R. Banghart, J. T. Williams, R. C. Shah, L. D. Lavis and B. L. Sabatini, *Mol. Pharmacol.*, 2013, **84**, 687–695.
28 C. J. Burnett and M. J. Krashes, *J. Neurosci. Off. J. Soc. Neurosci.*, 2016, **36**, 9268–9282.
29 S. M. Sternson and B. L. Roth, *Annu. Rev. Neurosci.*, 2014, **37**, 387–407.
30 D. M. O'Connor and N. M. Boulis, *Trends Mol. Med.*, 2015, **21**, 504–512.
31 J. Sevigny, P. Chiao, T. Bussière, P. H. Weinreb, L. Williams, M. Maier, R. Dunstan, S. Salloway, T. Chen, Y. Ling, J. O'Gorman, F. Qian, M. Arastu, M. Li, S. Chollate, M. S. Brennan, O. Quintero-Monzon, R. H. Scannevin, H. M. Arnold, T. Engber, K. Rhodes, J. Ferrero, Y. Hang, A. Mikulskis, J. Grimm, C. Hock, R. M. Nitsch and A. Sandrock, *Nature*, 2016, **537**, 50–56.
32 A. Canales, X. Jia, U. P. Froriep, R. A. Koppes, C. M. Tringides, J. Selvidge, C. Lu, C. Hou, L. Wei, Y. Fink and P. Anikeeva, *Nat. Biotechnol.*, 2015, **33**, 277–284.
33 J. W. Jeong, J. G. McCall, Y. Zhang, Y. Huang, M. R. Bruchas and J. A. Rogers, in *2015 Transducers - 2015 18th International Conference on Solid-State Sensors, Actuators and Microsystems (TRANSDUCERS)*, 2015, pp. 2264–2267.
34 M. HajjHassan, V. Chodavarapu and S. Musallam, *Sensors*, 2008, **8**, 6704–6726.
35 B. Fan and W. Li, *Lab Chip*, 2015, **15**, 3838–3855.
36 M. T. Alt, E. Fiedler, L. Rudmann, J. S. Ordonez, P. Ruther and T. Stieglitz, *Proc. IEEE*, 2017, **105**, 101–138.
37 P. Fattahi, G. Yang, G. Kim and M. R. Abidian, *Adv. Mater.*, 2014, **26**, 1846–1885.
38 A. Weltman, J. Yoo and E. Meng, *Micromachines*, 2016, **7**, 180.
39 G. Kook, S. W. Lee, H. C. Lee, I.-J. Cho and H. J. Lee, *Micromachines*, 2016, **7**, 179.
40 J. H. Lee, H. Kim, J. H. Kim and S.-H. Lee, *Lab Chip*, 2016, **16**, 959–976.
41 Outokumpu Oyj Inc., *Handbook of Stainless Steel*, Outokumpu Oyj, 2013.
42 M. A. Hopcroft, W. D. Nix and T. W. Kenny, *J. Microelectromech. Syst.*, 2010, **19**, 229–238.
43 W. Zhang, Y. Ma and Z. Li, *Med. Phys.*, 2016, **43**, 505–512.
44 A. Sridharan, J. K. Nguyen, J. R. Capadona and J. Muthuswamy, *J. Neural Eng.*, 2015, **12**, 36002.
45 H. Noh, K. Moon, A. Cannon, P. J. Hesketh, C. P. Wong and J. Micromechanics, *Microengineering*, 2004, **14**, 625.
46 P. J. Rousche, D. S. Pellinen, D. P. Pivin, J. C. Williams, R. J. Vetter and D. R. Kipke, *IEEE Trans. Biomed. Eng.*, 2001, **48**, 361–371.
47 Y. Sun, S. P. Lacour, R. A. Brooks, N. Rushton, J. Fawcett and R. E. Cameron, *J. Biomed. Mater. Res., Part A*, 2009, **90**, 648–655.
48 B. Rubehn and T. Stieglitz, *Biomaterials*, 2010, **31**, 3449–3458.
49 HD Microsystems Inc., *Material Data Sheet Polyimide PI 2525*, 2012.
50 Parylene Coating Services Inc., *Material Data Sheet Parylene*, 2011.
51 C. Y. Shih, T. A. Harder and Y. C. Tai, *Microsyst. Technol.*, 2004, **10**, 407–411.
52 C. Hassler, R. P. von Metzen, P. Ruther and T. Stieglitz, *J. Biomed. Mater. Res., Part B*, 2010, **93B**, 266–274.
53 B. Rubehn, C. Bosman, R. Oostenveld, P. Fries and T. Stieglitz, *J. Neural Eng.*, 2009, **6**, 36003.
54 N. Stark, *Med. Plast. Biomater.*, 1996, 30–35.
55 T. Stieglitz, M. Schuettler, B. Rubehn, T. Boretius, J. Badia and X. Navarro, in *2011 5th International IEEE/EMBS Conference on Neural Engineering (NER)*, 2011, pp. 529–533.
56 N. Lago, K. Yoshida, K. P. Koch and X. Navarro, *IEEE Trans. Biomed. Eng.*, 2007, **54**, 281–290.
57 F. E. H. Tay, J. A. van Kan, F. Watt, W. O. Choong and J. Micromechanics, *Microengineering*, 2001, **11**, 27.
58 H. Yu, O. Balogun, B. Li, T. W. Murray, X. Zhang and J. Micromechanics, *Microengineering*, 2004, **14**, 1576.
59 A. T. Al-Halhouli, I. Kampen, T. Krah and S. Büttgenbach, *Microelectron. Eng.*, 2008, **85**, 942–944.

60 M. Hopcroft, T. Kramer, G. Kim, K. Takashima, Y. Higo, D. Moore and J. Brugger, *Fatigue Fract. Eng. Mater. Struct.*, 2005, **28**, 735–742.
61 Microchem Inc., *Material Data Sheet SU-8 2000*, 2015.
62 L. J. Fernández, A. Altuna, M. Tijero, G. Gabriel, R. Villa, M. J. Rodríguez, Batlle Montse, R. Vilares, J. Berganzo and F. J. Blanco, *J. Micromech. Microeng.*, 2009, **19**, 25007.
63 G. Kotzar, M. Freas, P. Abel, A. Fleischman, S. Roy, C. Zorman, J. M. Moran and J. Melzak, *Biomaterials*, 2002, **23**, 2737–2750.
64 G. Voskerician, M. S. Shive, R. S. Shawgo, H. von Recum, J. M. Anderson, M. J. Cima and R. Langer, *Biomaterials*, 2003, **24**, 1959–1967.
65 K. V. Nemani, K. L. Moodie, J. B. Brennick, A. Su and B. Gimi, *Mater. Sci. Eng., C*, 2013, **33**, 4453–4459.
66 A. Altuna, G. Gabriel, L. M. de la Prida, M. Tijero, A. Guimerá, J. Berganzo, Salido Rafa, R. Villa and L. J. Fernández, *J. Micromech. Microeng.*, 2010, **20**, 64014.
67 A. Altuna, E. Bellistri, E. Cid, P. Aivar, B. Gal, J. Berganzo, G. Gabriel, A. Guimerà, R. Villa, L. J. Fernández and L. M. de la Prida, *Lab Chip*, 2013, **13**, 1422–1430.
68 S. Myllymaa, S. Pirinen, K. Myllymaa, M. Suvanto, T. A. Pakkanen, T. T. Pakkanen and R. Lappalainen, *Meas. Sci. Technol.*, 2012, **23**, 125701.
69 L. Guo, G. S. Guvanasen, X. Liu, C. Tuthill, T. R. Nichols and S. P. DeWeerth, *IEEE Trans. Biomed. Circuits Syst.*, 2013, **7**, 1–10.
70 S. R. Gutbrod, M. S. Sulkin, J. A. Rogers and I. R. Efimov, *Prog. Biophys. Mol. Biol.*, 2014, **115**, 244–251.
71 F. Abbasi, H. Mirzadeh and M. Simjoo, *J. Biomater. Sci., Polym. Ed.*, 2006, **17**, 341–355.
72 J. R. Capadona, D. J. Tyler, C. A. Zorman, S. J. Rowan and C. Weder, *MRS Bull.*, 2012, **37**, 581–589.
73 T. Kim, J. G. McCall, Y. H. Jung, X. Huang, E. R. Siuda, Y. Li, J. Song, Y. M. Song, H. A. Pao, R.-H. Kim, C. Lu, S. D. Lee, I.-S. Song, G. Shin, R. Al-Hasani, S. Kim, M. P. Tan, Y. Huang, F. G. Omenetto, J. A. Rogers and M. R. Bruchas, *Science*, 2013, **340**, 211–216.
74 B. Ziaie, A. Baldi, M. Lei, Y. Gu and R. A. Siegel, *Adv. Drug Delivery Rev.*, 2004, **56**, 145–172.
75 I. Papautsky, A. B. Frazier and H. Swerdlow, in *Proceedings IEEE The Tenth Annual International Workshop on Micro Electro Mechanical Systems. An Investigation of Micro Structures, Sensors, Actuators, Machines and Robots*, 1997, pp. 317–322.
76 L. Lin and A. P. Pisano, *J. Microelectromech. Syst.*, 1999, **8**, 78–84.
77 S. Chandrasekaran, J. D. Brazzle and A. B. Frazier, *J. Microelectromech. Syst.*, 2003, **12**, 281–288.
78 S. T. Retterer, K. L. Smith, C. S. Bjornsson, K. B. Neeves, A. J. H. Spence, J. N. Turner, W. Shain and M. S. Isaacson, *IEEE Trans. Biomed. Eng.*, 2004, **51**, 2063–2073.
79 K. B. Neeves, C. T. Lo, C. P. Foley, W. M. Saltzman and W. L. Olbricht, *J. Controlled Release*, 2006, **111**, 252–262.
80 K. Lee, J. He, R. Clement, S. Massia and B. Kim, *Biosens. Bioelectron.*, 2004, **20**, 404–407.
81 H. J. Lee, Y. Son, J. Kim, C. J. Lee, E.-S. Yoon and I.-J. Cho, *Lab Chip*, 2015, **15**, 1590–1597.
82 K. Seidl, S. Spieth, S. Herwik, J. Steigert, R. Zengerle, O. Paul, P. Ruther and J. Micromechanics, *Microengineering*, 2010, **20**, 105006.
83 M. J. de Boer, R. W. Tjerkstra, J. W. Berenschot, H. V. Jansen, G. J. Burger, J. G. E. Gardeniers, M. Elwenspoek and A. van den Berg, *J. Microelectromech. Syst.*, 2000, **9**, 94–103.
84 J. Chen, K. D. Wise, J. F. Hetke and S. C. Bledsoe, *IEEE Trans. Biomed. Eng.*, 1997, **44**, 760–769.
85 K. C. Cheung, K. Djupsund, Y. Dan and L. P. Lee, *J. Microelectromech. Syst.*, 2003, **12**, 179–184.
86 S.-J. Paik, A. Lee, K. Koo, S. Park, M. Jeong, H. Choi, J.-M. Lim, S. J. Oh, S. J. Kim and D. Cho, Localized stimulation and recording from neural cells with fluid injectable neuronal microneedles, *2005 9th International Conference on Miniaturized Systems for Chemistry and Life Science*, Boston, Massachusetts, USA, October 9–13, 2005, pp. 1177–1179.
87 J. John, Y. Li, J. Zhang, J. A. Loeb, Y. Xu and J. Micromechanics, *Microengineering*, 2011, **21**, 105011.
88 Z. Fekete, A. Pongrácz, P. Fürjes and G. Battistig, *Microsyst. Technol.*, 2012, **18**, 353–358.
89 Z. Fekete, A. Pongrácz, G. Márton and P. Fürjes, *Mater. Sci. Forum*, 2012, **729**, 210–215.
90 W. H. Lee, T. R. Slaney, R. W. Hower and R. T. Kennedy, *Anal. Chem.*, 2013, **85**, 3828–3831.
91 A. Pongrácz, Z. Fekete, G. Márton, Z. Bérces, I. Ulbert and P. Fürjes, *Sens. Actuators, B*, 2013, **189**, 97–105.
92 H. P. Neves, G. A. Orban, M. Koudelka-Hep, T. Stieglitz and P. Ruther, in *2007 3rd International IEEE/EMBS Conference on Neural Engineering*, 2007, pp. 104–109.
93 S. Spieth, O. Brett, K. Seidl, A. A. A. Aarts, M. A. Erismis, S. Herwik, F. Trenkle, S. Tätzner, J. Auber, M. Daub, H. P. Neves, R. Puers, O. Paul, P. Ruther, R. Zengerle and J. Micromechanics, *Microengineering*, 2011, **21**, 125001.
94 H. Shin, H. J. Lee, U. Chae, H. Kim, J. Kim, N. Choi, J. Woo, Y. Cho, C. J. Lee, E.-S. Yoon and I.-J. Cho, *Lab Chip*, 2015, **15**, 3730–3737.
95 D. Moser, K. Seidl, O. Paul and P. Ruther, in *2012 IEEE Sensors*, 2012, pp. 1–4.
96 S. Takeuchi, T. Suzuki, K. Mabuchi, H. Fujita and J. Micromechanics, *Microengineering*, 2004, **14**, 104.
97 B. J. Kim, J. T. W. Kuo, S. A. Hara, C. D. Lee, L. Yu, C. A. Gutierrez, T. Q. Hoang, V. Pikov and E. Meng, *J. Neural Eng.*, 2013, **10**, 45002.
98 S. T. Lin, M. Gheewala, J. C. Wolfe, J. A. Dani and W. C. Shih, in *2011 5th International IEEE/EMBS Conference on Neural Engineering (NER)*, 2011, pp. 700–703.
99 G. Márton, G. Orbán, M. Kiss, R. Fiáth, A. Pongrácz and I. Ulbert, *PLoS One*, 2015, **10**, e0145307.
100 A. Mercanzini, K. Cheung, D. L. Buhl, M. Boers, A. Maillard, P. Colin, J.-C. Bensadoun, A. Bertsch and P. Renaud, *Sens. Actuators, A*, 2008, **143**, 90–96.

101 H.-Y. Lai, L.-D. Liao, C.-T. Lin, J.-H. Hsu, X. He, Y.-Y. Chen, J.-Y. Chang, H.-F. Chen, S. Tsang and Y.-Y. I. Shih, *J. Neural Eng.*, 2012, **9**, 36001.
102 S. Yamagiwa, M. Ishida and T. Kawano, in *2015 Transducers - 2015 18th International Conference on Solid-State Sensors, Actuators and Microsystems (TRANSDUCERS)*, 2015, pp. 277–280.
103 Z. Xiang, S.-C. Yen, N. Xue, T. Sun, W. M. Tsang, S. Zhang, L.-D. Liao, N. V. Thakor and C. Lee, *J. Micromech. Microeng.*, 2014, **24**, 65015.
104 B. Y. Lee, J. Y. Jin, J. H. Park and J. Kim, in *2013 Transducers Eurosensors XXVII: The 17th International Conference on Solid-State Sensors, Actuators and Microsystems (TRANSDUCERS EUROSENSORS XXVII)*, 2013, pp. 321–324.
105 S. Metz, A. Bertsch, D. Bertrand and P. Renaud, *Biosens. Bioelectron.*, 2004, **19**, 1309–1318.
106 S. Takeuchi, D. Ziegler, Y. Yoshida, K. Mabuchi and T. Suzuki, *Lab Chip*, 2005, **5**, 519–523.
107 D. Ziegler, T. Suzuki and S. Takeuchi, *J. Microelectromech. Syst.*, 2006, **15**, 1477–1482.
108 A. Altuna, J. Berganzo and L. J. Fernández, *Frontiers in Materials*, 2015, **2**, 47.
109 Z. Xiang, H. Wang, S. Zhang, S.-C. Yen, M. Je, W. M. Tsang, Y.-P. Xu, N. V. Thakor, D.-L. Kwong and C. Lee, in *2013 8th IEEE International Conference on Nano/Micro Engineered and Molecular Systems (NEMS)*, 2013, pp. 1076–1079.
110 G. Petit-Pierre, A. Bertsch and P. Renaud, *Lab Chip*, 2016, **16**, 917–924.
111 P. Rohatgi, N. B. Langhals, D. R. Kipke and P. G. Patil, *Neurosurg. Focus*, 2009, **27**, E8.
112 S. Metz, R. Holzer and P. Renaud, *Lab Chip*, 2001, **1**, 29–34.
113 S. I. Park, D. S. Brenner, G. Shin, C. D. Morgan, B. A. Copits, H. U. Chung, M. Y. Pullen, K. N. Noh, S. Davidson, S. J. Oh, J. Yoon, K.-I. Jang, V. K. Samineni, M. Norman, J. G. Grajales-Reyes, S. K. Vogt, S. S. Sundaram, K. M. Wilson, J. S. Ha, R. Xu, T. Pan, T. Kim, Y. Huang, M. C. Montana, J. P. Golden, M. R. Bruchas, R. W. Gereau Iv and J. A. Rogers, *Nat. Biotechnol.*, 2015, **33**, 1280–1286.
114 J. G. McCall, T. Kim, G. Shin, X. Huang, Y. H. Jung, R. Al-Hasani, F. G. Omenetto, M. R. Bruchas and J. A. Rogers, *Nat. Protoc.*, 2013, **8**, 2413–2428.
115 C. Lu, U. P. Froriep, R. A. Koppes, A. Canales, V. Caggiano, J. Selvidge, E. Bizzi and P. Anikeeva, *Adv. Funct. Mater.*, 2014, **24**, 6594–6600.
116 H. E. Criswell, *Pharmacol., Biochem. Behav.*, 1977, **6**, 237–238.
117 M. A. Bozarth and R. A. Wise, *J. Neurosci. Methods*, 1980, **2**, 273–275.
118 S. Spieth, A. Schumacher, C. Kallenbach, S. Messner, R. Zengerle and J. Micromechanics, *Microengineering*, 2012, **22**, 65020.
119 A. Nisar, N. Afzulpurkar, B. Mahaisavariya and A. Tuantranont, *Sens. Actuators, B*, 2008, **130**, 917–942.
120 A. Cobo, R. Sheybani and E. Meng, *Adv. Healthcare Mater.*, 2015, **4**, 969–982.
121 S. R. Paul, S. K. Nayak, A. Anis and K. Pal, *Polym.-Plast. Technol. Eng.*, 2016, **55**, 965–975.
122 N.-C. Tsai and C.-Y. Sue, *Sens. Actuators, A*, 2007, **134**, 555–564.
123 E. Meng and T. Hoang, *Ther. Delivery*, 2012, **3**, 1457–1467.
124 E. S. Kim, E. Gustenhoven, M. J. Mescher, E. E. L. Pararas, K. A. Smith, A. J. Spencer, V. Tandon, J. T. Borenstein and J. Fiering, *Lab Chip*, 2014, **14**, 710–721.
125 W. Mamanee, A. Tuantranont, N. V. Afzulpurkar, N. Porntheerapat, S. Rahong and A. Wisitsoraat, *J. Phys.: Conf. Ser.*, 2006, **34**, 564.
126 P. S. Chee, M. N. Minjal, P. L. Leow and M. S. M. Ali, *Sens. Actuators, A*, 2015, **233**, 1–8.
127 N. A. Hamid, B. Y. Majlis, J. Yunas, A. R. Syafeeza, Y. C. Wong and M. Ibrahim, *Microsyst. Technol.*, 2016, 1–7.
128 N. A. Hamid, B. Y. Majlis, J. Yunas, A. A. Hamzah and M. M. Noor, *Adv. Sci. Lett.*, 2013, **19**, 2854–2859.
129 D. H. Jun, W. Y. Sim and S. S. Yang, *Sens. Actuators, A*, 2007, **139**, 210–215.
130 C. G. Cooney and B. C. Towe, *Sens. Actuators, A*, 2004, **116**, 519–524.
131 O. C. Jeong and S. S. Yang, *Sens. Actuators, A*, 2000, **83**, 249–255.
132 P. S. Chee, M. Nafea, P. L. Leow and M. S. M. Ali, *J. Mech. Sci. Technol.*, 2016, **30**, 2659–2665.
133 J. Fong, Z. Xiao and K. Takahata, *Lab Chip*, 2015, **15**, 1050–1058.
134 F. Sassa, Y. Al-Zain, T. Ginoza, S. Miyazaki and H. Suzuki, *Sens. Actuators, B*, 2012, **165**, 157–163.
135 F. Abhari, H. Jaafar and N. A. M. Yunus, *Int. J. Electrochem. Sci.*, 2012, **7**, 9765–9780.
136 M. S. M. Ali, K. Takahata and J. Micromechanics, *Microengineering*, 2011, **21**, 75005.
137 D. Xu, L. Wang, G. Ding, Y. Zhou, A. Yu and B. Cai, *Sens. Actuators, A*, 2001, **93**, 87–92.
138 W. L. Benard, H. Kahn, A. H. Heuer and M. A. Huff, *J. Microelectromech. Syst.*, 1998, **7**, 245–251.
139 B. Samel, P. Griss and G. Stemme, *J. Microelectromech. Syst.*, 2007, **16**, 50–57.
140 N. Roxhed, S. Rydholm, B. Samel, W. van der Wijngaart, P. Griss, G. Stemme and J. Micromechanics, *Microengineering*, 2006, **16**, 2740.
141 P. Griss, H. Andersson and G. Stemme, *Lab Chip*, 2002, **2**, 117–120.
142 S. Spieth, A. Schumacher, T. Holtzman, P. D. Rich, D. E. Theobald, J. W. Dalley, R. Nouna, S. Messner and R. Zengerle, *Biomed. Microdevices*, 2012, **14**, 799–809.
143 P.-Y. Li, J. Shih, R. Lo, S. Saati, R. Agrawal, M. S. Humayun, Y.-C. Tai and E. Meng, *Sens. Actuators, A*, 2008, **143**, 41–48.
144 P. Y. Li, R. Sheybani, J. T. W. Kuo and E. Meng, in *TRANSDUCERS 2009–2009 International Solid-State Sensors, Actuators and Microsystems Conference*, 2009, pp. 1461–1464.
145 A. Cobo, R. Sheybani, H. Tu and E. Meng, *Sens. Actuators, A*, 2016, **239**, 18–25.
146 R. Sheybani, A. Cobo and E. Meng, *Biomed. Microdevices*, 2015, **17**, 1–13.
147 R. Lo and E. Meng, in *2009 IEEE 22nd International Conference on Micro Electro Mechanical Systems*, 2009, pp. 236–239.

148 J. Oh, G. Kim, F. Kralick and H. Noh, *J. Microelectromech. Syst.*, 2011, **20**, 811–818.
149 J. J. Nagel, G. Mikhail, H. Noh and J. Koo, Magnetically actuated micropumps using an Fe-PDMS composite membrane, *Proc. SPIE, Smart Structures and Materials*, 2006, **6172**, 617213, DOI: 10.1117/12.658012.
150 C.-H. Cheng, C. Chao, Y.-N. Cheung, L. Xiao, M. Yang and W. Leung, in *2008 3rd IEEE International Conference on Nano/Micro Engineered and Molecular Systems*, 2008, pp. 1160–1163.
151 K. F. Chang, Y. C. Tsai, W. P. Shih and L. J. Yang, in *2010 IEEE 23rd International Conference on Micro Electro Mechanical Systems (MEMS)*, 2010, pp. 1039–1042.
152 W. Hilber, *Appl. Phys. A: Mater. Sci. Process.*, 2016, **122**, 751.
153 M. Fuchiwaki, Y. Naka and K. Tanaka, *Adv. Mater. Res.*, 2010, **93–94**, 615–618.
154 J. H. Kim, K. T. Lau, R. Shepherd, Y. Wu, G. Wallace and D. Diamond, *Sens. Actuators, A*, 2008, **148**, 239–244.
155 A. T. Evans, J. M. Park, S. Chiravuri and Y. B. Gianchandani, in *2008 IEEE 21st International Conference on Micro Electro Mechanical Systems*, 2008, pp. 252–255.
156 J. M. Park, A. T. Evans, K. Rasmussen, T. R. Brosten, G. F. Nellis, S. A. Klein and Y. B. Gianchandani, *J. Microelectromech. Syst.*, 2009, **18**, 868–877.
157 X. Wu, S.-H. Kim, C.-H. Ji and M. G. Allen, *J. Micromech. Microeng.*, 2011, **21**, 95003.
158 J. T. Santini, M. J. Cima and R. Langer, *Nature*, 1999, **397**, 335–338.
159 M. Staples, K. Daniel, M. J. Cima and R. Langer, *Pharm. Res.*, 2006, **23**, 847–863.
160 Y. Li, R. S. Shawgo, B. Tyler, P. T. Henderson, J. S. Vogel, A. Rosenberg, P. B. Storm, R. Langer, H. Brem and M. J. Cima, *J. Controlled Release*, 2004, **100**, 211–219.
161 Y. Li, H. L. H. Duc, B. Tyler, T. Williams, M. Tupper, R. Langer, H. Brem and M. J. Cima, *J. Controlled Release*, 2005, **106**, 138–145.
162 R. A. Scheidt, J. T. Santini, A. C. Richards, A. M. Johnson, A. Rosenberg, M. J. Cima and R. Langer, in *1st Annual International IEEE-EMBS Special Topic Conference on Microtechnologies in Medicine and Biology. Proceedings (Cat. No.00EX451)*, 2000, pp. 483–486.
163 J. M. Maloney, S. A. Uhland, B. F. Polito, N. F. Sheppard, C. M. Pelta and J. T. Santini, *J. Controlled Release*, 2005, **109**, 244–255.
164 J. H. Prescott, S. Lipka, S. Baldwin, N. F. Sheppard, J. M. Maloney, J. Coppeta, B. Yomtov, M. A. Staples and J. T. Santini, *Nat. Biotechnol.*, 2006, **24**, 437–438.
165 R. Goffredo, A. Ferrone, L. Maiolo, A. Pecora and D. Accoto, in *2015 37th Annual International Conference of the IEEE Engineering in Medicine and Biology Society (EMBC)*, 2015, pp. 3205–3208.
166 J. M. Portilla and U. Kim, in *2013 IEEE 26th International Conference on Micro Electro Mechanical Systems (MEMS)*, 2013, pp. 1077–1080.
167 N. M. Elman, H. L. H. Duc and M. J. Cima, *Biomed. Microdevices*, 2009, **11**, 625–631.
168 A. C. R. Grayson, I. S. Choi, B. M. Tyler, P. P. Wang, H. Brem, M. J. Cima and R. Langer, *Nat. Mater.*, 2003, **2**, 767–772.
169 Y. Li, N. Deng, X. Huang and S. Zhang, in *2015 16th International Conference on Electronic Packaging Technology (ICEPT)*, 2015, pp. 1233–1237.
170 P. J. Chang, Y. Y. Kao, M. L. Chan, M. Megens and D. A. Horsley, in *2012 IEEE Sensors*, 2012, pp. 1–4.
171 M. S. Groen, J. Groenesteijn, E. Meutstege, R. A. Brookhuis, D. M. Brouwer, J. C. Lötters and R. J. Wiegerink, *J. Microelectromech. Syst.*, 2015, **24**, 1759–1767.
172 A. J. Chung, B. Cordovez, N. Jasuja, D. J. Lee, X. T. Huang and D. Erickson, *Microfluid. Nanofluid.*, 2012, **13**, 345–352.
173 D. J. Cai, D. Aharoni, T. Shuman, J. Shobe, J. Biane, W. Song, B. Wei, M. Veshkini, M. La-Vu, J. Lou, S. E. Flores, I. Kim, Y. Sano, M. Zhou, K. Baumgaertel, A. Lavi, M. Kamata, M. Tuszynski, M. Mayford, P. Golshani and A. J. Silva, *Nature*, 2016, **534**, 115–118.
174 T. Ativanichayaphong, J. W. He, C. E. Hagains, Y. B. Peng and J.-C. Chiao, *J. Neurosci. Methods*, 2008, **170**, 25–34.
175 M. Alam, X. Chen and E. Fernandez, *J. Neural Eng.*, 2013, **10**, 66010.
176 C.-W. Chang and J.-C. Chiou, *Sensors*, 2013, **13**, 4624–4639.
177 S. I. Park, G. Shin, A. Banks, J. G. McCall, E. R. Siuda, M. J. Schmidt, H. U. Chung, K. N. Noh, J. G.-H. Mun, J. Rhodes, M. R. Bruchas and J. A. Rogers, *J. Neural Eng.*, 2015, **12**, 56002.
178 C. T. Wentz, J. G. Bernstein, P. Monahan, A. Guerra, A. Rodriguez and E. S. Boyden, *J. Neural Eng.*, 2011, **8**, 46021.
179 R. C. Pinnell, J. Dempster and J. Pratt, *J. Neural Eng.*, 2015, **12**, 66015.
180 A. J. Yeh, J. S. Ho, Y. Tanabe, E. Neofytou, R. E. Beygui and A. S. Y. Poon, *Appl. Phys. Lett.*, 2013, **103**, 163701.
181 G. Shin, A. M. Gomez, R. Al-Hasani, Y. R. Jeong, J. Kim, Z. Xie, A. Banks, S. M. Lee, S. Y. Han, C. J. Yoo, J.-L. Lee, S. H. Lee, J. Kurniawan, J. Tureb, Z. Guo, J. Yoon, S.-I. Park, S. Y. Bang, Y. Nam, M. C. Walicki, V. K. Samineni, A. D. Mickle, K. Lee, S. Y. Heo, J. G. McCall, T. Pan, L. Wang, X. Feng, T. Kim, J. K. Kim, Y. Li, Y. Huang, R. W. Gereau, J. S. Ha, M. R. Bruchas and J. A. Rogers, *Neuron*, 2017, **93**, 509–521.
182 M. Hashimoto, A. Hata, T. Miyata and H. Hirase, *Neurophotonics*, 2014, **1**, 011002.
183 Y. Iwai, S. Honda, H. Ozeki, M. Hashimoto and H. Hirase, *Neurosci. Res.*, 2011, **70**, 124–127.
184 V. Abinayaa and A. Jayan, Case Study on Comparison of Wireless Technologies in Industrial Applications, *International Journal of Scientific and Research Publications*, 2014, **4**, 1–4.
185 R. E. Hampson, V. Collins and S. A. Deadwyler, *J. Neurosci. Methods*, 2009, **182**, 195–204.
186 Y. Zatout, in *2012 IEEE 14th International Conference on e-Health Networking, Applications and Services (Healthcom)*, 2012, pp. 383–386.

187 G. Kim, H. Yun, M. Ryu, Y. Shin, H. Kim and Y. Yang, *Exp. Neurobiol.*, 2010, **19**, 165–172.
188 C.-K. Liang, J.-J. J. Chen, C.-L. Chung, C.-L. Cheng and C.-C. Wang, *Physiol. Meas.*, 2005, **26**, 83.
189 J. Yoo, L. Yan, S. Lee, Y. Kim, H. Kim, B. Kim and H. J. Yoo, in *2009 IEEE International Solid-State Circuits Conference – Digest of Technical Papers*, 2009, pp. 290–291.
190 D. A. Borton, M. Yin, J. Aceros and A. Nurmikko, *J. Neural Eng.*, 2013, **10**, 26010.
191 S.-H. Song, G. T. Gillies, M. A. Howard, B. Kuhnley and M. Utz, *Biomed. Microdevices*, 2013, **15**, 27–36.
192 H. Kassiri, A. Bagheri, N. Soltani, K. Abdelhalim, H. M. Jafari, M. T. Salam, J. L. P. Velazquez and R. Genov, in *ESSCIRC 2014 – 40th European Solid State Circuits Conference (ESSCIRC)*, 2014, pp. 95–98.
193 R. Jegadeesan, N. V. Thakor and S. C. Yen, in *2015 7th International IEEE/EMBS Conference on Neural Engineering (NER)*, 2015, pp. 648–651.
194 A. K. RamRakhyani, S. Mirabbasi and M. Chiao, *IEEE Trans. Biomed. Circuits Syst.*, 2011, **5**, 48–63.
195 X. Li, H. Zhang, F. Peng, Y. Li, T. Yang, B. Wang and D. Fang, *Sensors*, 2012, **12**, 10292–10308.
196 B. H. Waters, A. P. Sample, P. Bonde and J. R. Smith, *Proc. IEEE*, 2012, **100**, 138–149.
197 R. F. Xue, K. W. Cheng and M. Je, *IEEE Trans. Circuits Syst. Regul. Pap.*, 2013, **60**, 867–874.
198 H. Li, J. Li, K. Wang, W. Chen and X. Yang, *IEEE Trans. Power Electron.*, 2015, **30**, 3998–4008.
199 C. A. Balanis, *Antenna Theory: Analysis and Design, 3rd Edition*, Wiley-Interscience, Hoboken, NJ, 3rd edn, 2005.
200 S. I. Park, G. Shin, J. G. McCall, R. Al-Hasani, A. Norris, L. Xia, D. S. Brenner, K. N. Noh, S. Y. Bang, D. L. Bhatti, K.-I. Jang, S.-K. Kang, A. D. Mickle, G. Dussor, T. J. Price, R. W. Gereau, M. R. Bruchas and J. A. Rogers, *Proc. Natl. Acad. Sci. U. S. A.*, 2016, 201611769.
201 S. I. Park, *Prog. Electromagn. Res.*, 2013, **135**, 123–136.
202 R. Farra, N. F. Sheppard, L. McCabe, R. M. Neer, J. M. Anderson, J. T. Santini, M. J. Cima and R. Langer, *Sci. Transl. Med.*, 2012, **4**, 122ra21.
203 B. P. Timko, M. Arruebo, S. A. Shankarappa, J. B. McAlvin, O. S. Okonkwo, B. Mizrahi, C. F. Stefanescu, L. Gomez, J. Zhu, A. Zhu, J. Santamaria, R. Langer and D. S. Kohane, *Proc. Natl. Acad. Sci. U. S. A.*, 2014, **111**, 1349–1354.
204 T. Hoare, J. Santamaria, G. F. Goya, S. Irusta, D. Lin, S. Lau, R. Padera, R. Langer and D. S. Kohane, *Nano Lett.*, 2009, **9**, 3651–3657.
205 T. Hoare, B. P. Timko, J. Santamaria, G. F. Goya, S. Irusta, S. Lau, C. F. Stefanescu, D. Lin, R. Langer and D. S. Kohane, *Nano Lett.*, 2011, **11**, 1395–1400.
206 I. Banerjee, R. C. Pangule and R. S. Kane, *Adv. Mater.*, 2011, **23**, 690–718.
207 C. Blaszykowski, S. Sheikh and M. Thompson, *Chem. Soc. Rev.*, 2012, **41**, 5599–5612.
208 B. G. Reuben, O. Perl, N. L. Morgan, P. Stratford, L. Y. Dudley and C. Hawes, *J. Chem. Technol. Biotechnol.*, 1995, **63**, 85–91.
209 D. J. H. Tng, R. Hu, P. Song, I. Roy and K.-T. Yong, *Micromachines*, 2012, **3**, 615–631.
210 H. Zhang and M. Chiao, *J. Med. Biol. Eng.*, 2015, **35**, 143–155.
211 B. W. Kristensen, J. Noraberg, P. Thiébaud, M. Koudelka-Hep and J. Zimmer, *Brain Res.*, 2001, **896**, 1–17.
212 L. Yang, L. Li, Q. Tu, L. Ren, Y. Zhang, X. Wang, Z. Zhang, W. Liu, L. Xin and J. Wang, *Anal. Chem.*, 2010, **82**, 6430–6439.
213 C. Zhao, L. Li, Q. Wang, Q. Yu and J. Zheng, *Langmuir*, 2011, **27**, 4906–4913.
214 Z. Wu, W. Tong, W. Jiang, X. Liu, Y. Wang and H. Chen, *Colloids Surf., B*, 2012, **96**, 37–43.
215 Y.-N. Zhou, Z.-H. Luo and J.-H. Chen, *AIChE J.*, 2013, **59**, 3019–3033.
216 Y. Li, A. J. Keefe, M. Giarmarco, N. D. Brault and S. Jiang, *Langmuir*, 2012, **28**, 9707–9713.
217 A. J. Keefe, N. D. Brault and S. Jiang, *Biomacromolecules*, 2012, **13**, 1683–1687.
218 Q. Tu, J.-C. Wang, Y. Zhang, R. Liu, W. Liu, L. Ren, S. Shen, J. Xu, L. Zhao and J. Wang, *Rev. Anal. Chem.*, 2012, **31**, 177–192.
219 J. Zhou, D. A. Khodakov, A. V. Ellis and N. H. Voelcker, *Electrophoresis*, 2012, **33**, 89–104.
220 C. Yuan, J. Gao, J. Guo, L. Bai, C. Marshall, Z. Cai, L. Wang and M. Xiao, *PLoS One*, 2014, **9**, e107447.
221 N. Philippe, M. Legendre, G. Doutre, Y. Couté, O. Poirot, M. Lescot, D. Arslan, V. Seltzer, L. Bertaux, C. Bruley, J. Garin, J.-M. Claverie and C. Abergel, *Science*, 2013, **341**, 281–286.
222 I. Gitlin, J. D. Carbeck and G. M. Whitesides, *Angew. Chem., Int. Ed.*, 2006, **45**, 3022–3060.
223 S. Deshayes, M. C. Morris, G. Divita and F. Heitz, *Cell. Mol. Life Sci.*, 2005, **62**, 1839–1849.
224 R. A. Barker, J. Barrett, S. L. Mason and A. Björklund, *Lancet Neurol.*, 2013, **12**, 84–91.
225 M. B. Victor, M. Richner, T. O. Hermanstyne, J. L. Ransdell, C. Sobieski, P.-Y. Deng, V. A. Klyachko, J. M. Nerbonne and A. S. Yoo, *Neuron*, 2014, **84**, 311–323.
226 M. Richner, M. B. Victor, Y. Liu, D. Abernathy and A. S. Yoo, *Nat. Protoc.*, 2015, **10**, 1543–1555.
227 H. Haug, *Am. J. Anat.*, 1987, **180**, 126–142.
228 A. A. Grace and S. P. Onn, *J. Neurosci. Off. J. Soc. Neurosci.*, 1989, **9**, 3463–3481.
229 M. J. Hoogduijn, J. C. van den Beukel, L. C. M. Wiersma and J. Ijzer, *BMJ*, 2013, **347**, f6833.
230 J. Ge, L. Guo, S. Wang, Y. Zhang, T. Cai, R. C. H. Zhao and Y. Wu, *Stem Cell Rev. Rep.*, 2014, **10**, 295–303.
231 E. Dressaire and A. Sauret, *Soft Matter*, 2016, **13**, 37–48.
232 S. S. Massenburg, E. Amstad and D. A. Weitz, *Microfluid. Nanofluid.*, 2016, **20**, 94.
233 A. Geipel, F. Goldschmidtboeing, P. Jantscheff, N. Esser, U. Massing and P. Woias, *Biomed. Microdevices*, 2008, **10**, 469–478.
234 K. Junwu, Y. Zhigang, P. Taijiang, C. Guangming and W. Boda, *Sens. Actuators, A*, 2005, **121**, 156–161.

235 E. R. Siuda, J. G. McCall, R. Al-Hasani, G. Shin, S. Il Park, M. J. Schmidt, S. L. Anderson, W. J. Planer, J. A. Rogers and M. R. Bruchas, *Nat. Commun.*, 2015, **6**, 8480.
236 R. Al-Hasani, J. G. McCall, G. Shin, A. M. Gomez, G. P. Schmitz, J. M. Bernardi, C.-O. Pyo, S. I. Park, C. M. Marcinkiewcz, N. A. Crowley, M. J. Krashes, B. B. Lowell, T. L. Kash, J. A. Rogers and M. R. Bruchas, *Neuron*, 2015, **87**, 1063–1077.
237 J. R. Capadona, K. Shanmuganathan, D. J. Tyler, S. J. Rowan and C. Weder, *Science*, 2008, **319**, 1370–1374.
238 T. Ware, D. Simon, C. Liu, T. Musa, S. Vasudevan, A. Sloan, E. W. Keefer, R. L. Rennaker and W. Voit, *J. Biomed. Mater. Res., Part B*, 2014, **102**, 1–11.
239 I. M. Van Meerbeek, B. C. Mac Murray, J. W. Kim, S. S. Robinson, P. X. Zou, M. N. Silberstein and R. F. Shepherd, *Adv. Mater.*, 2016, **28**, 2801–2806.
240 A. Balasubramanian, M. Standish and C. J. Bettinger, *Adv. Funct. Mater.*, 2014, **24**, 4860–4866.
241 I. Tochitsky, M. R. Banghart, A. Mourot, J. Z. Yao, B. Gaub, R. H. Kramer and D. Trauner, *Nat. Chem.*, 2012, **4**, 105–111.
242 J. A. Frank, D. A. Yushchenko, D. J. Hodson, N. Lipstein, J. Nagpal, G. A. Rutter, J.-S. Rhee, A. Gottschalk, N. Brose, C. Schultz and D. Trauner, *Nat. Chem. Biol.*, 2016, **12**, 755–762.
243 M. Banghart, K. Borges, E. Isacoff, D. Trauner and R. H. Kramer, *Nat. Neurosci.*, 2004, **7**, 1381–1386.
244 L. K. Massey, *Permeability Properties of Plastics and Elastomers, 2nd Ed.: A Guide to Packaging and Barrier Materials*, Cambridge University Press, 2003.
245 S. J. Metz, *PhD Thesis*, University of Twente, 2003.
246 Accuratus Ceramic Inc., *Handbook of Fused Silica Material Properties*, Accuratus Ceramic, 2013.
247 M. Tilli, T. Motooka, V.-M. Airaksinen, S. Franssila, M. Paulasto-Krockel and V. Lindroos, *Handbook of Silicon Based MEMS Materials and Technologies*, William Andrew, 2015.
248 J. Kim, A. Banks, Z. Xie, S. Y. Heo, P. Gutruf, J. W. Lee, S. Xu, K.-I. Jang, F. Liu, G. Brown, J. Choi, J. H. Kim, X. Feng, Y. Huang, U. Paik and J. A. Rogers, *Adv. Funct. Mater.*, 2015, **25**, 4761–4767.
249 K. M. Musick, J. Rigosa, S. Narasimhan, S. Wurth, M. Capogrosso, D. J. Chew, J. W. Fawcett, S. Micera and S. P. Lacour, *Sci. Rep.*, 2015, **5**, 14363.
250 C. Hassler, T. Boretius and T. Stieglitz, *J. Polym. Sci., Part B: Polym. Phys.*, 2011, **49**, 18–33.
251 Dow Corning Corporation, *Material Data Sheet, Sylgard ® 184 Silicone*, Dow Corning Inc., 2014.
252 P. S. Nunes, P. D. Ohlsson, O. Ordeig and J. P. Kutter, *Microfluid. Nanofluid.*, 2010, **9**, 145–161.
253 IDEX Health & Science LLC, *Life Sciences Polymer Materials*, IDEX Corporation, 2017.